

3D CAPACITANCE EXTRACTION WITH THE METHOD OF MOMENTS

by

TAO LI

A Thesis
Submitted to the Faculty
of the
WORCESTER POLYTECHNIC INSTITUTE
in partial fulfillment of the requirements for the
Degree of Master of Science
in
Electrical and Computer Engineering
by

01/2010

APPROVED:

Professor Sergey N. Makarov, Major Advisor

Professor Reinhold Ludwig

Professor Alexander E. Emanuel

Abstract

In this thesis, the Method of Moments has been applied to calculate capacitance between two arbitrary 3D metal conductors or a capacitance matrix for a 3D multi-conductor system.

Capacitance extraction has found extensive use for systems involving sets of long parallel transmission lines in multi-dielectric environment as well as integrated circuit package including three-dimensional conductors located on parallel planes. This paper starts by reviewing fundamental aspects of transient electro-magnetics followed by the governing differential and integral equations to motivate the application of numerical methods as Method of Moments(MoM), Finite Element Method(FEM), etc. Among these numerical tools, the surface-based integral-equation methodology - MoM is ideally suited to address the problem. It leads to a well-conditioned system with reduced size, as compared to volumetric methods. In this dissertation, the MoM Surface Integral Equation (SIE)-based modeling approach is developed to realize electrostatic capacitance extraction for 3D geometry. MATLAB is employed to validate its efficiency and effectiveness along with design of a friendly GUI.

As a base example, a parallel-plate capacitor is considered. We evaluate the accuracy of the method by comparison with FEM simulations as well as the corresponding quasi-analytical solution. We apply this method to the parallel-plate square capacitor and demonstrate how far could the undergraduate result ' $C = A * \epsilon / d$ ' be from reality. For the completion of the solver, the same method is applied to the calculation of line capacitance for two- and multi-conductor 2D transmission lines.

Acknowledgements

I would like to express my gratitude to all those who gave me the possibility to complete this Thesis.

My deepest gratitude goes first and foremost to Professor Sergey N. Makarov, my supervisor whose help, stimulating suggestions and encouragement helped me in all the time of research for and writing of this Thesis. Without him, this Thesis would not have been possible.

I am grateful to my former adviser Professor Yunxiang Xie, who introduced and helped me to start my graduate student life in Electrical Engineering. His visionary thoughts and energetic working style have greatly influenced me.

I thank the rest of my thesis committee members: Professor Reinhold Ludwig and Professor Alexander Emanuel. Their valuable feedback helped me to improve the dissertation in many ways.

I thank all the students and staffs in Electrical and Computer Engineering department, whose presence and fun-loving spirits made the otherwise grueling experience tolerable. Special thanks to my friends who gave me their ears when I complained and their minds when I asked for help during the course of this difficult Thesis. They are Zanzan Zhu, Chen Shen, Artem Saitgareev, Di Pu, Sijing Shen, Linxi Shi and Yanjie Peng. I also would like to thank all the group members in Antenna Lab: Vishwanath Iyer and Eduardo M.A. Oliveira. I enjoyed all the vivid discussions we had on various topics and had lots of fun being a member of this fantastic group.

Last, my thanks would go to my beloved family for their loving considerations and great confidence in me all through these years. They have been always there when I needed them most, and for supporting me through times thin and thick.

Contents

List of Figures	vi
List of Tables	vii
List of Symbols	viii
1 Introduction	1
1.1 Motivation of This Work	1
1.2 Comparison of Differential Equation Method and Integral Equation Method	2
1.3 Application and Development of MoM in Electromagnetic problem	5
1.3.1 General formulations of MoM	5
1.3.2 Development of MoM	6
1.4 Problem statement	8
1.5 Chapter Abstract	9
2 Full Wave Equations and Static Approximation	11
2.1 Maxwell's equations	11
2.1.1 Dynamic Case	11
2.1.2 Phasor form	12
2.1.3 Quasi-static Case	13
2.1.4 Static Case	14
2.2 Use of potentials	14
2.3 Solution to Maxwell equation	15
2.3.1 Full wave solution	15
2.3.2 Simplified solution	17
2.3.3 Boundary Relation	19
2.4 Electric Field and Capacitance	20
3 Static Capacitance Extraction By Means of Moment of Method	24
3.1 Calculation of potential integrals involving the scalar Green function and its gradient	25
3.2 MoM application to Metal geometry in free space	26
3.2.1 MoM equations	27
3.2.2 Integral calculation	30

3.2.3	Charge Conservation Law	33
3.3	MoM approach to conductor with dielectric layer	33
3.3.1	Poisson's equation	34
3.3.2	Multi-conductor transmission line in a multilayered dielectric region above infinity ground plane	35
3.3.3	2D Multiconductor transmission line in a multilayered dielectric re- gion with finite-ground plane	39
3.4	Conclusion	40
4	MATLAB Implementation and Numerical results	42
4.1	GUI Design with MATLAB	42
4.2	Matrix calculation in MATLAB	45
4.3	Mesh refinement and Convergence discussion	46
4.3.1	Adaptively refined mesh	47
4.3.2	Convergence standard	49
4.4	2D Numerical examples	51
4.4.1	Coupled micro-strip line	51
4.4.2	Coupled strip line between parallel conducting planes	52
4.4.3	Quadline	52
4.5	3D numerical example	55
4.5.1	AMAZE - Finite Element Method	56
4.5.2	Analytic solution based BEM	59
4.5.3	MoMtool	60
4.6	Conclusion	64
5	Conclusion	65
A	List of Abbreviation	66
B	Capacitance of Parallel-plate Square Capacitor	68
	Bibliography	70

List of Figures

1.1	Solving Poisson's Equation for Complex 3D Structures	10
3.1	Surface triangular mesh	28
4.1	MainMenu	43
4.2	2D Mesh Interface	43
4.3	3D Mesh Interface	44
4.4	Trangle rendering using adaptive subdivision	48
4.5	Coupled micro-strips	51
4.6	Coupled stip line	52
4.7	Quad-line moedel in Ansoft and MoMtool	53
4.8	An error between Ansoft 3D results and MoMtool 2D results	54
4.9	Convergence comparison between Ansoft andMoMtool (eps.r=8, d/w=0.363)	54
4.10	Parallel-plate square capacitor	55
4.11	Electric field of Parallel-plate Square Cpacitor in FEM	58
4.12	Boundary study of FEM	58
4.13	Capacitance of Parallel-plate capacitor using FEM model	60
4.14	Capacitance of Parallel-plate capacitor using BEM model	61
4.15	Parallel-plate Capacitor defined in MoMtool	62
4.16	Charge density distribution of Parallel-plate Capacitor	62
4.17	Capacitance of Parallel-plate Capacitor	63
4.18	Error between different numerical results	63
4.19	Curve fitting based on MoM result	64
B.1	Capacitance of Parallel-plate square capacitor	69

List of Tables

4.1	Results comparison of coupled micro-strip line	51
4.2	Results comparison of coupled strip line	52
4.3	Capacitance of Parallel-plate Capacitor	61
A.1	List of Abbreviation	67

List of Symbols

δ	Delta-function
λ_j	The simplex coordinates on the source triangle
μ	Magnetic permeability [N/m^2]
ω	Angular frequency [rad/s]
ω_n	Testing function of MoM equations
\vec{A}	Magnetic vector potential [Wb/m]
\vec{B}	Magnetic flux density [$N \cdot A/m^3(Tesla)$]
\vec{D}	Displacement/Electric flux density [C/m^2]
\vec{E}	Electric field [V/m]
\vec{H}	Magnetic field [pA/m]
\vec{J}	Conduction current density [A/m^2]
\vec{r}	Position vector of integration point
\vec{r}'	Position vector of observation point
Φ	Electric potential [V]
ρ	Volumetric electric charge density [C/m^3]
ρ_s	Surface charge density [C/m^2]

σ	Conductivity [S/m]
\underline{C}	Capacitance matrix
ε	Electric permittivity [F/m]
ε_0	Electric permittivity in free space [F/m]
φ_{spec}	Electrostatic potential [V]
A	Area of the triangle [m^2]
a_n	Unknown coefficient in MoM equations
b	Fringing field index
C	Capacitance [F]
c_i	Center of the triangle or midpoint edge position
$e^{j\omega t}$	Complex exponential form
$G(\vec{r}, \vec{r}')$	Free Space Green's Function
h_n	Edge length [m]
L	Inductance [$H(\Omega \cdot s)$]
l	Integral line of a surface
N_c	Number of perfect conductor
N_d	Number of dielectric layers
Q	Total conductor charge [C]
r_i	Corners of the triangle
S	A closed surface around the conductor
s_n	Expansion function or basis function of MoM equations

V	Voltage vector [V]
Z	MoM matrix
k	Wave number0 [m^{-1}]

Chapter 1

Introduction

1.1 Motivation of This Work

Ever since 1970's, increased interest existed in the computation of the capacitance coefficients in multi-conductor systems[62, 56, 26, 33]. With the development of very large-scale integration (VLSI) in the realm of high-speed digital and microwave circuits, faster and more accurate calculations for the capacitance and inductance matrices of complex multi-conductor structures in multilayer media is in demand[53, 29, 68]. The knowledge of the self and coupling capacitance can help the designer to optimize the layout of the circuit. For example, the interconnection of delay time caused by parasitic RC (resistance and capacitance) or to make a more accurate estimation of capacitance for the design of better motion sensors. In some cases, knowledge of the coupling parameters is absolutely critical. For example, coupling coefficients are essential in predicting the amount of cross-talk noise in high-density coupled interconnect lines. Hence, parasitic parameter extraction turns to be a key factor and needs to be investigated thoroughly.

Advances in integrated circuit technology in the microwave region also necessitate a sophisticated analysis, design, and construction of transmission lines[35, 62, 64, 6]. All electrical parameters required for a complete characterization of a set of low-loss transmission lines are obtainable based on the calculation of the static capacitance of transmission line system[14]. For a transmission line, only one cross-section of the line is usually of inter-

est, which is perpendicular to the z-axis. The field and charge distribution remains the same for any cross-section. Thus transmission line model is always solved in 2D case. The analysis of microcircuit interconnections has also been performed by transmission line techniques which can be solved as 2D problem. However, with the development of complicated circuit package and conductor geometry, 3D capacitance extraction is necessary for many applications. Two typical examples of complicated three-dimensional structures, for which capacitance strongly affects performance, are dynamic memory cells and the chip carriers commonly used in high-density packaging[70]. All these reasons have increased interest in computationally efficient procedures for determining capacitance of general two-dimensional or three-dimensional structures.

The useful result of an electromagnetic field analysis for a static configuration or a uniform transmission line is often a prediction of the capacitance and inductance. The usual procedure is to: first, determine the relevant charge or field flux density by solving a boundary value problem, and then integrate the density to get the total charge or flux. Finally, capacitance is the ratio of total charge to applied voltage, and inductance is the ratio of magnetic flux (linkages) to current [23]. Field calculation is not a limitation and is undesirable as long as the rigorous field analysis can be carried through in closed form [15, 21]. However, in many important problems most conductors are irregular in shapes and finite in dimension which is sufficiently complicated that an analytical closed-form solution is not obtainable. Since an electromagnetic field can be determined by a differential equation or integral equation formulation, the most straightforward way to obtain an approximate solution of the integral equation is through direct application of numerical techniques[67].

1.2 Comparison of Differential Equation Method and Integral Equation Method

Many numerical methods have been applied to extract the electrical parameters of the interconnects and packages. These methods can be generally classified into two categories: differential equation methods and integral equation methods. The common features of these methods include discretization of the unknown function, approximations, and the solution

based on matrix solution techniques. The approximations result in inaccuracies[20].

The differential equation methods, such as Finite Element Method(FEM) and Finite Difference Method(FDM)[20] divide an interconnect cell into meshes and lead to a large scale sparse matrix equation. Two types of basis functions used in FEM are node-based and edge-based. Node-based functions are commonly used for simplicity of analysis. The numerical calculation of electrostatic fields requires the solution of a large set of coupled linear equations, one for each active node in the solution volume which require the set up of boundary condition for the whole solution volume. [46][47] present an accurate and efficient method for extraction of parasitic capacitance in sub micron integrated circuits. The method uses a 3-D finite element model in which the conductor charges are approximated by a piece-wise linear function on a web of edges located on the surface of the conductors. This yields a system of Green's function integral equations that is solved by a novel approximate matrix inversion technique. [69]also gives a 3D capacitance extraction utilizing FDM method. Though the compressed storage technique and some efficient sparse matrix equation solvers maybe applied, the solving process is still time-consuming and needs vast memory resources.

The integral equation methods, such as the Method of Moments(MoM) and the Boundary Element Method(BEM), divides the surfaces of conductors and the interfaces of dielectric layers into meshes and lead to a comparatively smaller but full matrix. This procedure is robust [37]and has many advantages over finite difference or finite element schemes, including good conditioning, reduction in dimensionality, and the ability of treating arbitrary regions. However, when the number of conductors and dielectric layers increase, the analysis procedure will also be too costly in terms of computing time and memory needs due to high cost of working with large dense matrix. Therefore, while the numerical solution of the IE delivers good performance in the a two-dimensional analysis[54], its application in three-dimensional capacitance extraction have been limited to small problems. Solutions have been obtained for problems involving infinite dielectric regions [49, 18] by using Green's function techniques similar to those used in the two-dimensional calculations.

It is well known that none of these methods is the most efficient in all cases. [20] listed the qualitative comparison of computational methods. And [38] generalized different

application conditions for FEM and MoM ,

- The MoM is more convenient for open problems than the FEM, and vice versa,
- The MoM/SIE is well suited for wire and plate structures, while the MoM/VIE and the FEM are well suited for dielectric structures
- The MoM matrices are always full. while the FEM matrices are sparse:
- The MoM is more efficient in the case of small problems, while FEM is more efficient in the case of large problems

However, these application rules are not always correct.

As we can see from above, all the algorithms suffer from at least one limitation. In order to overcome this difficulty, Hybrid method combined differential methods and integral methods. The result was a good trend for 3D capacitance extraction development to keep good accuracy with enlarged application range of 3D geometries For example,[65] presents a new algorithm of coupling computation of BEM and the finite difference method (FDM) to avoid a significant error that occurs if some dielectrics do not contain a conductor. This algorithm still uses BEM for dielectrics which contain conductors, but employs FDM for those without. The numerical results indicate that this algorithm reduces calculation error greatly. [68] utilizes the element-by-element (EBE) technique in finite element method (FEM) for the solution of electric field, together with preconditioned conjugate gradient (PCG) solver for solving large matrix equation. It can be used for fast parameter extraction of multi-layer and multi-conductor interconnects in VLSI circuit. Compared to some reference solutions, both the memory requirement and the CPU time are significantly reduced while maintaining a relatively high accuracy.

1.3 Application and Development of MoM in Electromagnetic problem

1.3.1 General formulations of MoM

The MoM is a powerful and versatile numerical method for the solution of partial integral equations. A global overview can be found in[20]. Applications of MoM to electromagnetics are discussed in many recent papers since 1970's. Before we go any further, we will give the general formulations of MoM.

Considering the inhomogeneous equation:

$$\zeta(f) = g \quad (1.1)$$

where ζ is a linear operator, g is known and f is to be determined, we shall now perform the two essential steps.

1. Let f be expanded in a series of functions:

$$f = \sum a_n s_n \quad (1.2)$$

where a_n are constant. The set s_n is called expansion function, or basis functions. Note that for an exact solution, the summation should be taken to ∞ , but has to be truncated in practice.

2. It is assumed that a suitable inner product has been defined for the problem. Now, we define a set of weighting functions, or testing functions, $\omega_1, \omega_2, \dots, \omega_N$ in the range of ζ , and take the inner product of the previous equation with $\omega_1, \omega_2, \dots, \omega_N$.

$$\sum \alpha_n \langle \omega_m, \zeta f_1 \rangle = \langle \omega_m, g \rangle \quad (1.3)$$

The system can now be written in matrix form as:

$$[A_{mn}] [a_n] = [g_m] \quad (1.4)$$

$$\text{where } [A_{mn}] = \begin{bmatrix} \langle \omega_1, \zeta f_1 \rangle & \langle \omega_1, \zeta f_2 \rangle & \cdots \\ \langle \omega_2, \zeta f_1 \rangle & \langle \omega_2, \zeta f_2 \rangle & \cdots \\ \cdots & \cdots & \ddots \end{bmatrix}, [a_n] = \begin{bmatrix} a_1 \\ a_2 \\ a_3 \end{bmatrix}, [g_m] = \begin{bmatrix} \langle \omega_1, \zeta f_1 \rangle \\ \langle \omega_2, \zeta f_1 \rangle \\ \vdots \end{bmatrix}$$

If the matrix $[A_{mn}]$ is not singular, the unknowns α_n are simply given by:

$$[a_n] = [A_{mn}]^{-1} [g_{mn}] \quad (1.5)$$

and the original function f can be reconstructed using Eq.(1.2). We can now generalize the following definitions:

The basis functions used previously are defined as:

$$s_n = \begin{cases} 1 & \text{if } x \text{ belongs to the interval } n \\ 0 & \text{otherwise} \end{cases} \quad (1.6)$$

The testing (or weighting functions):

Point matching = taking Dirac functions δ as testing functions.

The advantage of the MoM over purely numerical methods is that there is still a large part that remains analytic like the Green's functions [20]. Yet, it remains a numerical method based on a matrix inversion technique and therefore, convergence issues need to be examined. The convergence of the MoM is closely related to the choice of basis functions and, although to a lesser extent, to the choice of testing functions. There are essentially two families of basis functions: entire domain basis functions yielding a good convergence of the method without mesh process and sub-domain basis functions rely on a proper meshing of the geometry giving more flexibility of the geometry[39]. Finally, we can mention that point matching, which is easy to grasp and straightforward to implement, may not yield an optimal convergence. In most of the applications, the Galerkin technique is better, which consists in choosing the same testing functions as the basis functions[27]. This applies to both sub-domain and entire domain functions.

1.3.2 Development of MoM

MoM involves a good amount of preprocessing of Maxwell's equations because it makes use of the Green's function[20]. It's proposed as a surface-based integral-equation methodology. It leads to a well-conditioned system with reduced size, as compared to volumetric methods [38], but the system of equations generated is inherently dense, thereby creating

a time and memory bottleneck. Several fast iterative techniques have been developed to efficiently solve and solve a MoM system with linear time and memory complexity. All these methods, including QR-based approaches[37][22], fast-multipole methods (FMMs) [44], and FFT-based techniques [50] etc.

[37]gave the QR-based fast iterative solver (IES3) which adopts a binary tree multi-level decomposition of the geometry and consequent low-rank compression of the MoM sub-matrices which represent the interaction between well-separated geometrical regions. This scheme is particularly attractive for circuit problems.[22]presents an improved matrix-compression technique for fast iterative solution of such dense systems, which applies QR decomposition on multilevel Oct-tree-based interaction sub-matrices. It combined the regular-tree structure of the fast-multipole method with the rank-revealing QR-based matrix-compression scheme to achieve superior time and memory efficiency. As is demonstrated by the numerical-simulation results presented herein, the new algorithm is found to be faster and more memory efficient than both existing QR-based methods and FastCap. The fast multipole method (FMM) [24], while originally developed for particle simulation problems, can be combined with iterative techniques to solve the dense integral equation matrices that arise from the Laplace equation. Parameter extraction programs such as FastCap[44] and FastHenry[36] use the FMM for accelerating the dense matrix-vector products required by an iterative solver. FastCap and FastHenry[44, 43] employ the FMM that was originally developed for particle simulation problems.

Focusing on decreasing the load for computer to do the matrix calculation, several other methods based on MoM were presented. One of the most powerful methods for the efficient MoM solution is the multilevel fast multipole algorithm (MLFMA)[12][25, 59, 58] [17], which marries the fast multipole method (FMM) [24]and a multi-level multi-grid interpolation concept [9]. It can largely reduce the computational complexity and memory requirement of the matrix calculation. Another powerful method for the efficient MoM solution is the adaptive integral method[10] (AIM) that has been developed by Bleszynski et al., [8]. Compared to the conventional MoM, AIM reduces computational complexity and memory requirement with the aid of auxiliary basis functions and fast Fourier transform (FFT) that is used in the Precorrected-FFT method[50] . The AIM has been successfully applied to the anal-

ysis of scattering by, and radiation from, arbitrarily shaped three-dimensional and planar structures [60, 41, 8]. Refer[10] apply the AIM to calculate the capacitance matrix for an arbitrarily shaped 3D structure and the memory requirement and computational complexity proved its effectiveness of computing capacitance of an arbitrarily shaped 3D structure. The solutions introduced in Refer[10] considerably reduce storage requirements for the matrix of coefficients without unduly increasing computation complexity, allowing the treatment of three-dimensional conductors on multiple planes and Refer[29] presented a new capacitance extraction method named Dimension Reduction Technique for 3D VLSI interconnects. It converts a complex 3D problem into a series of cascading simple 2D problems.

1.4 Problem statement

Given different choice, any EM or RF problem can be solved, in principle, using full Maxwell's equations; subject to the corresponding boundary conditions. However, in many cases the solution of full Maxwell's equations is very cumbersome. Based on application environment, different simplifications can be made that yield an almost identical result. Therefore, in numerical modeling applications, different EM and RF software packages use different approximations depending on a specific problem under study[19]. For example: magnetostatic and eddy-current models for power electronics[28], electrostatics model for transmission lines[12], electrostatics model for semiconductor modeling or full wave solution for antenna modeling[57], etc.

Until now, several commercial as well as public domain tools such as TMA's Raphael(based on Finite Difference Method (FDM)), Ansoft's SPICELINK(based on Finite Element Method (FEM)) and MIT's FastCap (based on multipole accelerated Boundary Element Method (BEM)) are available to calculate the statistic capacitance of various interconnects. Then, considering the transmission line, since the transverse electric fields of a TEM mode (the fields in the xy-plane whilst the wave propagates along the z-axis) are curl-free (have the electric potential) and satisfy Laplace's equation in the domain with no charges[14], similar observation is valid for the transverse magnetic fields, with the charges residing on metal conductors, the Laplace's equation for the corresponding electric potential φ is trans-

formed to the well-known Poisson's equation. This circumstance allows us to find the static capacitance per unit length between two or more conductors using established numerical or analytical electrostatic techniques. The analytical techniques are based on conformal mapping in 2D space (transformation to a complex plane and contour reduction) - see, for example, Ref.[14].

Therefore, the task of this paper is to utilize MoM to calculate the capacitance matrix of arbitrarily shaped conductors embedded in multiple dielectric regions with a static model. The multi-conductor system is analyzed under different conditions. It could be situated over a finite or infinite ground plane, or could be between two ground planes. The solution is useful for finding characteristic impedance or equivalent circuits of microstrip junctions as well as discontinuities and for vias connecting conductors located in various dielectric regions. Some of the conductors may be of finite volume and others may be infinitely thin. Even though a large volume of literature exists to analyze an infinitely long transmission line, there are very few satisfactory procedures to solve for the equivalent circuits of junctions and vias connecting conductors located in various dielectric layers.

1.5 Chapter Abstract

In Chapter 2, the Maxwell's equation is reviewed and Green's function is presented to show the relation between charge density and potential for the conductor. Also, certain boundary condition is explained as basis to solve the system including dielectric layers.

In Chapter 3, principle of MoM is reviewed then the formulation of the IE solution is developed. MoM equations of multi-conductor system under different conditions are discussed and the evaluation of the capacitance coefficient matrix is considered.

In Chapter 4, MoM solution is implemented with MATLAB code. Fig.(1.1) shows its general information. Results of several numerical examples are provided to do the comparison with analytical solution or existing numerical solution utilizing other numerical method. Furthermore, numerical facts influencing the effectiveness and accuracy are generalized.

Problem

Capacitance extraction based on the accurate solution of Poisson's equation for multiple-conductor systems

Present Approach

Moment of Method with triangular mesh
Single-point Gaussian integration
Adaptive mesh refinement

Strengths

Triangular mesh treats complex geometry
Faster calculation speed with SIE/MoM for metal conductor system

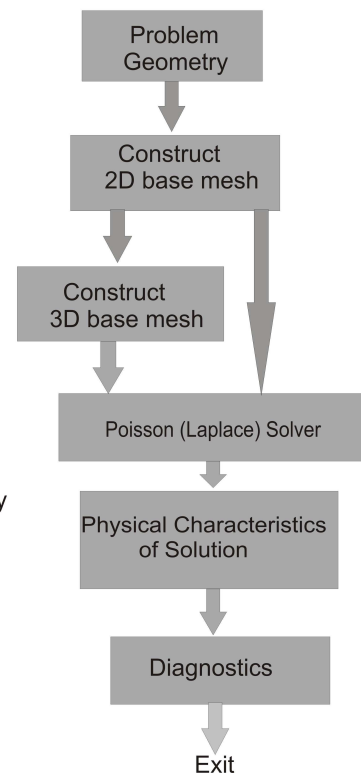


Figure 1.1: Solving Poisson's Equation for Complex 3D Structures

Chapter 2

Full Wave Equations and Static Approximation

This chapter reviews the Maxwell equations in the context of modeling the electromagnetic behavior of a metallic structure. Starting from the full wave equations and its simplified forms, potential formulations are reviewed which require fewer unknowns to be solved than the full set of Maxwell equations. The quasi-static approximation is motivated and the static approximation is presented. Basic field theory is given in order to clarify which field variables are mandatory in order to clarify which further simplifications could be carried out. When possible, respective field solutions are introduced. While Numerical methods are treated in chapters to follow, they will reference back to the theory presented here.

2.1 Maxwell's equations

2.1.1 Dynamic Case

The most fundamental equations of classical electrodynamics are the Maxwell equations which consist of a system of coupled partial differential equations. Consider a medium with electric permittivity ε and magnetic permeability μ and with no (fictitious) magnetic current density. The sources are given by (volumetric) conduction current density J and by

volumetric electric charge density ρ . Then, Maxwell's equations for electric field intensity \vec{D} and magnetic field intensity \vec{B} have the form [67]

Gauss' law for electric field

$$\nabla \cdot \vec{D} = \rho \quad (2.1)$$

Faraday's law

$$\nabla \times \vec{E} = -\frac{\partial \vec{B}}{\partial t} \quad (2.2)$$

Gauss' law for magnetic field (no magnetic charges)

$$\nabla \cdot \vec{B} = 0 \quad (2.3)$$

Ampere's law modified by displacement currents

$$\nabla \times \vec{H} = -\frac{\partial \vec{D}}{\partial t} + \vec{J} \quad (2.4)$$

Material relations as Eq.(2.5) exist which relate the magnetic flux density to magnetic field, electric displacement current to electrical field and electric current density to electric field

$$\vec{B} = \mu \vec{H}, \vec{D} = \epsilon \vec{E}, \vec{J} = \sigma \vec{E} \quad (2.5)$$

where μ is the relative permeability, ϵ is the relative permittivity, σ is conductivity.

Eqs.(2.1)-(2.4) together with Eq.(2.6), is the basic set of equations of classical electricity and magnetism, governing all electromagnetic phenomena in the range of frequencies from zero through the highest-frequency radio waves and in the range of sizes above atomic size.

2.1.2 Phasor form

Considering the majority of engineering applications utilize steady state AC fields varying sinusoidally in time, and also that transients or time variations of other forms which by the method of Fourier analysis[30] maybe considered a superposition of such steady-state sinusoids of different frequency, there is advantages to use the complex exponential form($e^{j\omega t}$). As Eq.(2.6)shows, the time periodic behavior of all field variables f is assumed.

$$f(\vec{r}, t) = \Re[\hat{f}(\vec{r})e^{j\omega t}] \quad (2.6)$$

Note that only the real part of the phasor representation has a physical meaning and the complex number carries the phase information. Therefore, to find the frequency domain solution, formally the set of Eq.(2.1)-(2.4) are easily changed over by replacing $\frac{\partial}{\partial t}$ by $j\omega$:

$$\nabla \cdot \vec{D} = \rho \quad (2.7)$$

$$\nabla \times \vec{E} = -j\omega \vec{B} \quad (2.8)$$

$$\nabla \cdot \vec{B} = 0 \quad (2.9)$$

$$\nabla \times \vec{H} = -j\omega \vec{D} + \vec{J} \quad (2.10)$$

The basic prerequisite for such a substitution is the linearity of Maxwell's equations.

2.1.3 Quasi-static Case

The quasi-static case differs from the fully dynamic case only by its neglect of the displacement current. It happens when:

$$\sigma \gg \omega \varepsilon \quad (2.11)$$

Eq.(2.11) is fulfilled in conducting media for even high frequencies, because $\varepsilon_0 = 8.85 \cdot 10^{-12}[F/m]$ is a small number and the electrical conductivity of metals is typically $\sigma > 10^7[S/m]$. Within this approximation, the time derivative of the displacement current $\partial D/\partial t$ in Eq.(2.4) is discarded leading to

$$\nabla \times \vec{H} = \vec{J} \quad (2.12)$$

and that Eq.(2.1)-(2.3) are still holding. Since the divergence of the curl of a vector is zero, we see from that in the quasi-static case,

$$\nabla \cdot \vec{J} = 0 \quad (2.13)$$

The quasi-static approximation reduces the mathematical complexity of the Maxwell equations and leads to results with sufficient accuracy. It is used for time-varying fields in many conducting media. This is because, for good conductors, the conduction current greatly exceeds the displacement current for frequencies that usually concern us (right up to X-ray frequencies). A good example of this is the calculation of time-varying magnetic fields in iron cores, the so-called “eddy-current” problem[32]. This has practical applications in electric motors, generators, magnetic recording heads, and solenoid actuators.

2.1.4 Static Case

In the static case, both the electric displacement current and the time-varying magnetic flux density are neglected, which means in static approximation all time dependence of the Maxwell equations Eq.(2.1)-(2.4) is neglected. In the frequency domain this corresponds to $\omega = 0$. Furthermore, since there is no phase delay due to alternating current, all field variables become real. Note that electric and magnetic fields are completely decoupled[19]. In this case Eq.(2.2) becomes:

$$\nabla \times \vec{E} = 0 \quad (2.14)$$

In addition to these equations, Eq.(2.1),(2.3) and Eq.(2.13) still hold. Static field calculations are made wherever the dictates of physical reality permit, because, as we will see below, they are of relative simplicity compared to dynamic and quasi-static calculations. As an example, many calculations in the magnetic fields of magnets are static calculations.

2.2 Use of potentials

In order to determine the field generated by a given source: like antennas, waveguides, cavity excitations, etc, the solution is easier to obtain if we introduce auxiliary vector potential function Φ (electric potential) and \vec{A} magnetic vector potential[31].

The magnetic vector potential \vec{A} is defined with Eq.(2.11)

$$\vec{B} = \nabla \times \vec{A} \quad (2.15)$$

It fulfills Eq.(2.2) automatically, because $\nabla \cdot (\nabla \times f) = 0$ for any vector field f . Equation (2.15), however, does not yield a unique definition for \vec{A} , because the gradient of a scalar field $\nabla\Phi$ can be added without change of the curl of the sum. Useful definitions of \vec{A} depend on respective approximations of the Maxwell equations and are given below[?].

From Eq.(2.7) and (2.11) it follows that

$$\nabla \times \vec{E} = -j\omega \nabla \times \vec{A} \quad (2.16)$$

The curl operator is applied to both sides of Eq.(2.16). The difference between fields \vec{E} and \vec{A} can hence be only the gradient of a scalar field, e.g. $\nabla\Phi$,

$$\vec{E} = -j\omega \vec{A} - \nabla\Phi \quad (2.17)$$

2.3 Solution to Maxwell equation

Electromagnetic fields at a point may be determined using Faraday's law Eq.(2.1) Amperé's law Eq.(2.3), constitutive relations, and boundary conditions directly which is followed in the finite-difference time-domain(FDTD) method[20]. However, the most convenient approach to determine the steady state fields is to solve the wave equations, which are derived from Eq.(2.6).

2.3.1 Full wave solution

With Eq.(2.1) and material relation Eq.(2.5) it follows that;

$$\nabla \cdot \vec{E} = -j\omega \nabla \cdot \vec{A} - \Delta\Phi = \frac{\rho}{\epsilon} \quad (2.18)$$

Note that during derivation of Eq.(2.18), the dielectric permittivity has been set constant in space. In order to solve for a complete field distribution, solutions in domains with each constant dielectric permittivity have to be matched at the domain boundaries. For matching conditions cf. [31]. With use of the vector identity[19], the curl of the magnetic field in Eq.2.4 can be written as

$$\nabla \times \vec{H} = \frac{1}{\mu}(\nabla \nabla \vec{A} - \Delta \vec{A}) \quad (2.19)$$

Note that in Eq.(2.19) the magnetic permeability has been set constant as assumed in Sec. 2.1. Eq.(2.4) is reformulated with Eq.(2.17) and (2.2).

$$\nabla \nabla \vec{A} - \Delta \vec{A} = \mu \vec{J} + \mu \varepsilon (\omega^2 \vec{A} - \nabla \Phi) \quad (2.20)$$

The Helmholtz Theorem states that vector fields are defined when both curl and divergence are defined. Here, the "Lorentz Gauge" as [31]

$$\nabla \cdot \vec{A} = -j\omega \varepsilon \mu \Phi \quad (2.21)$$

is a useful definition of the divergence of . Eq. (2.18)simplifies to

$$\Delta \Phi + \omega^2 \varepsilon \mu \Phi = -\frac{\rho}{\varepsilon} \quad (2.22)$$

and Eq.(2.20) becomes

$$\Delta \vec{A} + \mu \varepsilon \omega^2 \vec{A} = -\mu \vec{J} \quad (2.23)$$

Equations (2.22) and (2.23) are both inhomogeneous Helmholtz equations with one and three components, respectively. Solutions can be obtained with use of Green's function G

$$(\Delta + k^2)G(\vec{r}, \vec{r}') = -4\pi\delta(\vec{r} - \vec{r}') \quad (2.24)$$

Where , $k^2 = \omega^2 \varepsilon \mu$, δ stands for the delta-function and

$$G^\pm(\vec{r}, \vec{r}') = \frac{e^{\pm jk|\vec{r}-\vec{r}'|}}{|\vec{r} - \vec{r}'|} \quad (2.25)$$

In Eq.(2.25) the plus-minus sign denotes expanding and contracting waves respectively. This can be deduced from the full solution in time, which is given by

$$G^\pm(\vec{r}, \vec{r}') = G^\pm(\vec{r}, \vec{r}')e^{j\omega t} \quad (2.26)$$

With the "plus" sign and increasing time, the phase argument $+k(\vec{r} - \vec{r}') + \omega t$ stays constant when the distance $|\vec{r} - \vec{r}'|$ decreases. Hence the "plus"-sign corresponds to incoming waves. The "minus"-sign leads to inverse behavior and hence corresponds to outgoing waves. Since initially fields are zero at infinity, only outgoing waves and hence only the "minus" sign is considered during the following analysis.

The full inhomogeneous solution of Eq.(2.22) is calculated by superposition of Green's functions,

$$\Phi(\vec{r}) = \frac{1}{4\pi} \int_V \frac{\rho(\vec{r}') e^{-jk|\vec{r} - \vec{r}'|}}{|\vec{r} - \vec{r}'|} d^3 r' \quad (2.27)$$

The same holds for the three solutions (one for every coordinate direction) of Eq. (2.23)

$$A_i(\vec{r}) = \frac{1}{4\pi} \int_V \frac{J_i(\vec{r}') e^{-jk|\vec{r} - \vec{r}'|}}{|\vec{r} - \vec{r}'|} d^3 r' \quad (2.28)$$

Where $i = x, y, z$ denotes the respective coordinate direction. When current and charge densities are given, computation of a field solution with Eq.(2.27) and (2.28) is straight forward. However, since the electromagnetic contact behavior is typically characterized by S-parameters or impedance values, current and charge densities have to be computed too, when either the electric potentials at contacts or the total conductor currents are known.

In order to solve for the three unknown components of $\vec{J}(\vec{r})$ and the unknown field $\rho(\vec{r})$, four additional equations are required. The current density $\vec{J}(\vec{r})$ can be calculated with Eq.(2.17) and material relation Eq.(2.5). The charge density $\rho(\vec{r})$ can be calculated from the continuity equation

$$\nabla \cdot \vec{J}(\vec{r}) + j\omega\rho(\vec{r}) = 0 \quad (2.29)$$

which always has to be fulfilled[55]. Use of Eq.(2.29) however introduces a coupling into Eq.(2.27) and (2.28). Therefore these equations cannot be solved independently.

2.3.2 Simplified solution

The quasi-static approximation reduces the mathematical complexity of the Maxwell equations and leads to results with sufficient accuracy, when certain conditions are met as

we discussed in section 2.1.3. To get simplified solution with quasi-static approximation, we must follow the same steps as we did in Sec.2.3.1. The simplification leads to a difference in Eq.(2.20),

$$\nabla\nabla\vec{A} - \Delta\vec{A} = \mu\vec{J} \quad (2.30)$$

Here, the "Coulomb Gauge"[31] $\nabla\cdot\vec{A} = 0$ is better suited for adjustment of $\nabla\vec{A}$ Equation(2.18) then reduces to

$$\Delta\Phi = -\frac{\rho}{\varepsilon} \quad (2.31)$$

as Poisson's equation and Eq.(2.30) becomes

$$\Delta\vec{A} = -\mu\vec{J} \quad (2.32)$$

Both equations are inhomogeneous Laplace equations and can be solved with use of Green's functions

$$\Delta\vec{G}(\vec{r}, \vec{r}') = -4\pi\delta(\vec{r} - \vec{r}') \quad (2.33)$$

where in this case $\vec{G}(\vec{r}, \vec{r}') = \frac{1}{|\vec{r} - \vec{r}'|}$.

The difference between Eq.(2.25) and Eq.(2.33) is the missing retardation term $e^{-jk|\vec{r} - \vec{r}'|}$; which accounts for the wave propagation delay in case of the full wave solution. Since there is no wave propagation delay within the quasi-static approximation, the wave velocity appears to be infinite. Obviously this approximation yields good results when the wavelength is large compared to the conductor dimensions.

As in the previous section, fields Φ and \vec{A} can be calculated directly when charge and currents are known,

$$\Phi(\vec{r}) = \frac{1}{4\pi} \int_V \frac{\rho(\vec{r}')}{|\vec{r} - \vec{r}'|} d^3r' \quad (2.34)$$

and for the three coordinate directions separately

$$A_i(\vec{r}) = \frac{1}{4\pi} \int_V \frac{J_i(\vec{r}')}{|\vec{r} - \vec{r}'|} d^3 r' \quad (2.35)$$

where $i = x, y, z$ denotes the respective coordinate direction.

One more simplification can be applied when considering that electric and magnetic field are "basically" decoupled within this approximation[48]. Generally electric and magnetic fields are coupled, because one field can be determined from the other by Eq.(2.2) and (2.4). However when time derivatives become smaller due to small coupling, this task becomes increasingly difficult to perform (by means of measurements or from numerical simulation results). It is therefore a common engineering approach [48] to simulate (and measure) electric and magnetic field independently. Note, that still only limited theoretical foundation is available for this decoupling behavior in case of general geometries. When applying the static approximation as we stated in section 2.1.4, the electric and magnetic fields are completely decoupled. The electric field can be characterized with capacitance values as in the quasi-static approximation.

2.3.3 Boundary Relation

In a single medium the electric field is continuous. However, at the boundary between two different media, the electric field may change abruptly both in magnitude and direction. It is of great importance in many problems to know the relations of the fields at such boundaries. These boundaries are discussed in many books. Boundary problem is discussed in two parts: the relation between the fields tangent to the boundary and the fields normal to the boundary. The tangential components of the electric field are the same on both sides of a boundary between two dielectrics. Meanwhile, by using flux density \vec{D} , we can get Eq.(2.36) from Gauss's law,

$$D_{n1} - D_{n2} = \rho_s \quad (2.36)$$

Where D_{n1} denotes the average flux density normal to the upper side of boundary in medium1 and D_{n2} denotes the average flux density normal to the bottom side of boundary in medium2, ρ_s denotes the surface charge density on the boundary. ρ_s is usually zero at a

dielectric-dielectric boundary unless charge has been placed there by mechanical means, as by rubbing. If the boundary is free from charge, $\rho_s=0$ and Eq.(2.36) reduces to

$$D_{n1} = D_{n2} \quad (2.37)$$

If medium 2 is conductor, Eq.(2.37) reduces to

$$D_{n1} = \rho_s \quad (2.38)$$

It is important to note that ρ_s in these relations refers to actual electric charge separated by finite distances from equal quantities of opposite charge and not to surface charge due to polarization.

2.4 Electric Field and Capacitance

This section describes the calculation of the electric field and capacitance[31][40]. With appropriate boundary conditions, the electric field can be described with a capacitance value. Several ways are presented to compute a capacitance value. When $\vec{B} = 0$ it follows from Eqs.(2.15) and (2.17) that $\vec{A} = 0$. The electric field can now be calculated from the scalar potential alone.

$$\vec{E} = -\nabla\Phi \quad (2.39)$$

From Eq.(2.27) it is known that Φ depends entirely on ρ . For an over-all characterization of the field for a given potential the capacitance

$$C = \frac{Q}{V} \quad (2.40)$$

can be used. In Eq.(2.40) Q denotes the total conductor charge and V denotes the respective constant potential between conductor and infinity. The total conductor charge can be calculated with Gauss' law

$$Q = \int_S -\epsilon\nabla\Phi dS \quad (2.41)$$

Where S is a closed surface around the conductor and dS denotes the outward normal on S . Because of the constant conductor potential, inside conductors $\rho = 0$. This is true for frequencies where metals serve as electric conductors. Conductors are separated by insulators where also $\rho = 0$. Therefore the Laplace equation Eq. (2.31) has to be solved with $\Phi = 1V$ on the conductor surface and $0V$ at infinity

$$\Delta\Phi(\vec{r}') = 0 \quad (2.42)$$

Note that with non-constant dielectric permittivity Eq. (2.41) becomes [31]

$$\nabla\varepsilon(\vec{r}')\nabla\Phi(\vec{r}') = 0 \quad (2.43)$$

The capacitive behavior of a multi-conductor system is described by a capacitance matrix \underline{C} with

$$\underline{C}V = Q \quad (2.44)$$

In Eq.(2.44), V denotes the vector of conductor potentials and Q denotes the vector of total conductor charges. Capacitance matrix entries C_{ij} correspond to charges accumulated on conductor j , when an electric potential of $1V$ is applied to conductor i and all other conductors are kept at zero potential. Note that only the inverse relation Eq.(2.27) between charge and potential is available directly. In fact, there are two other interrelated definitions of the capacitance matrix for multiconductor lines. Here, we consider only the so-called Maxwellian capacitance matrix explained as above [56][64].

Written Eq.(2.44) to matrix form as Eq.(2.45), the ij th element of the Maxwell capacitance matrix is the free charge on the i th conductor when the potential of the j th conductor is $1V$ and all other conductors are grounded. In [64], the elements of the Maxwellian capacitance matrix are called coefficients of capacitance. All coefficients of capacitance in Eq.(2.45) are determined directly from the MoM analysis which will be discussed in the next chapter.

$$\begin{aligned}
Q_1 &= C_{11}V_1 + C_{12}V_2 + \cdots + C_{1N}V_N \\
Q_2 &= C_{21}V_1 + C_{22}V_2 + \cdots + C_{2N}V_N \\
&\dots \\
Q_3 &= C_{N1}V_1 + C_{N2}V_2 + \cdots + C_{NN}V_N
\end{aligned} \tag{2.45}$$

The inductance matrix L_{ij} is called L . According to Ref. [14], the ij th element of L is the magnetic flux passing between a unit length of the i th conductor and the lower ground plane when one ampere of net z -directed electric current flows on the j th conductor and there is no net z -directed electric current on any of the other conductors. Here, z is the coordinate perpendicular to the xy plane. It can be shown that :

$$L = \mu_0 \varepsilon_0 [C_0]^{-1} \tag{2.46}$$

where C_0 is the ground capacitance matrix in vacuum of the same transmission line with the dielectric being removed.

According to [5], entries in the capacitance matrix \underline{C} have the following features:

1. Since Eq.2.45 is symmetric in i and j , also C is symmetric, i.e. $C_{ij} = C_{ji}$.
2. $C_{ij} > 0 \forall i$. When conductor i is placed at some positive potential and all other conductors are placed at zero potential, conductor i must carry a positive charge.
3. $C_{ij} < 0 \forall j \neq i$. When all other conductors are placed at zero potential, they must carry a negative charge. Hence, all entries in C generally are non zero. Conductors can be shielded by covering them with a material with high dielectric permittivity.
4. $\sum_j C_{ij} \geq 0 \forall i$. The sum of capacitance matrix entries in row i equals the sum of all conductor charges, when 1V electric potential is applied to conductor i and 0V is applied to all other conductors. Between conductors, the electric displacement current is divergence free. Hence the sum of flux integrals Eq(2.31) is zero, when there exists an outer boundary around the system of conductors with no electric field penetration. The sum is greater than zero, when electric field flux emanates towards

infinity. When the sum of row entries vanishes, the capacitance matrix is singular, because one column can be determined from the other columns.

5. \underline{C} is positive definite, because the electric field energy $\frac{1}{2}V^T CV > 0 \forall V \neq 0$.
6. When different conductor i and j are electrically connected and thus a new conductor with index is formed, the reduced capacitance matrix \tilde{C} can be computed by setting potentials and all other conductor potentials to $0V$. The new diagonal entry can be calculated from the total conductor charge. It is given by $\tilde{C}_{\lambda\lambda} = C_{ii} + C_{jj} + C_{ij} + C_{ji}$. Off diagonal entries are given by $C_{\lambda k} = C_{ik} + C_{jk}$.

Similar to calculation of electric field and capacitance, magnetic field and inductance can be deduced based on Equations stated in above sections. Also for multi-conductor system, entries in the inductance matrix L have the similar features as capacitance matrix \underline{C} [40]

Chapter 3

Static Capacitance Extraction By Means of Moment of Method

After the basic review of the Maxwell equation in Chapter2, this chapter will present a method to compute the electrostatic capacitance matrix for a multi-conductor system in free space or multiple dielectric regions. We will follow a classic references text refer[49, 56, 16, 61], which will be compared to finite element method currently widely used by commercial software packages such as HFSS Ansoft and Amaze. The formulation is obtained by using a free-space Green's function in conjunction with total charge on the conductor-to-dielectric interfaces and polarization charge on the dielectric-to-dielectric interfaces. The solution is effected by the method of moments using triangular sub-domains with piecewise constant expansion functions and point matching for testing.

As stated in Chapter1, the basic difference between the analysis of transmission lines and junctions of lines, vias, etc., is that for the former case we are solving a two-dimensional problem and, for the latter case, we are solving a three-dimensional problem. In this chapter we will include MoM application to both 2D and 3D geometry. This chapter is organized as follows: Section 3.1 describes the method to calculate the potential integral required in MoM. Section 3.2 describes the MoM equations for modeling the pure metal structure in free space. Section 3.3 describes the MoM equations for the conductors embedded in dielectric layers with proper boundary conditions for Dielectric-to-dielectric interface and

conductor-to-dielectric interface. Section 3.4 makes a conclusion of MoM modeling for multi-conductor system and propose possible numerical improvement for current modeling. Numerical results are presented for some typical multi-conductor systems in chapter 4.

3.1 Calculation of potential integrals involving the scalar Green function and its gradient

Evaluations of the integrals involving the Green's function kernel and its derivative are important in the numerical implementation of the electric-field integral equations (EFIE)[51, 66, 4]. Ever since 1970's, Green's function-integral equation approach [52, 35, 49] has been used explicitly to find the capacitance coefficients for a system of irregular finite conductors on a dielectric sheet. There are two parts to the Green's function-integral equation approach considered herein: the first deals with a derivation of Green's functions for a desired mathematical model; the second solves the integral equation by a discretization procedure in which a solution for a large number of unknowns is required - a significant limitation. This approach, however, allows treatment of rather complex finite geometric configurations that are useful in the design of modern thin circuits. Different methods are used to solve the integral equation.

Over the past several decades, many approaches have been presented[49, 51, 66, 23, 16, 4] to handle double surface potential integrals, based on triangular basis functions. [49] follows the integral transformation whose mathematical objective is to reduce a difficult problem in the original domain to a simpler form[20]. It utilized Fourier integral expression to express Green's function. One may construct the desired Green's functions by superposition in this way. Solution can be found for different cases easily considering different boundary conditions for different dielectric regions and ground plane. [51] presented a complete analytical integration to eliminate the need for special treatment of the singular integrals which arise for the diagonal elements of the matrix. It also sidesteps the question of what order numerical quadrature is required to integrate over any given triangular-shaped region. Preliminary tests have indicated that analytical evaluation of the integrals is also more efficient than numerical integration. However, this solution has limitations when the triangle forms a

right angle which needs to be solved in another way. [66] gives a detailed analysis about the integral calculation for uniform and linear source distributions on polygonal and polyhedral domains. Corresponding analytic solutions are given in detail for reference. As an extension of [23], [61] presents a semi-analytical method for computing the quasi-static double surface potential integrals, arising in the boundary integral (BI) models of electrically very small objects and for static electromagnetic-field computation.

In this paper, we prefer to use the simplest midpoint numerical integration for singular potential integrals, even though the analytical integration, or a more accurate numerical integration, are both possible for the static 2D or 3D problem [6, 3]. The analysis assumes a uniform charge over each subarea, the results should approach the theoretical value if the number of subareas are increased indefinitely. However, the computation time increases very rapidly for large number of subareas. Thus adaptive mesh refinement is applied to improve the accuracy of integral calculation with more basis functions (fine mesh) in the domains with large charge density and less basis functions (coarse mesh) in the domains with small charge density while still keep the higher efficiency acquired from one-point integral method. Midpoint numerical integration will fail for singular self-coupling terms as you will see from section 1.2.2, so the analytical solution generalized in [16] will be used.

Although it is generally true that the use of smoother basis functions enhances the convergence of the solution for closed surfaces with continuous normals, for general arbitrary shaped surfaces having corners or edges where the charge may be singular, the lack of continuity of the simple pulse functions turns out to be an advantage since pulses actually model the singular behavior better.

3.2 MoM application to Metal geometry in free space

As simple start of electrostatic modeling for multi-conductor system, in this section, the MoM equation for a pure metal system with finite-ground or ground at infinite distance is derived and solved for the EFIE, utilizing the pulse function as basis function, and δ function as testing function. Also there are concerns for the ground plane in multi-conductor systems. There are three cases:

1. Multi-Conductor systems with finite-ground
2. Multi-Conductor systems above infinity ground
3. Multi-Conductor systems with ground in finite distance

In this chapter, all of them will be discussed but the numerical results will be only given under condition (1) and (3).

There are different ways to deal with these conditions:

1. By meshing both plates(i.e, meshing everything ,which is of course always possible in finite region). This will yield bigger matrix and more unknown values in the MoM equation
2. By using the image theory, and declaring the new problem is equivalent to the one of a unique plate on top of a ground plane. In this case, we only have to change the Green's function to take the ground plane into account, and we keep less number of unknowns in MoM equations. When possible, this solution is better because computationally less expensive (analytically more expensive)

Basically, a general trend is to have a Green's function that represents as much as possible of the environment and to mesh only those parts that are external to the environment. This is in fact the reason why people are looking for Green's functions in layered media, periodic media, etc.

3.2.1 MoM equations

Consider a multi-conductors system with a finite common ground in free space as shown in Fig.3.1. Since in metal conductors, charges only reside on their surfaces, but not in the volume, with reference to Fig3.1a, the surface integral in Eq.(2.34) over the metal surface $S = S_1 + S_2 + \dots + S_N$ need to be solved. Following by two steps of MoM decribed in section 1.3.1:

1. Mesh the structure: divide the surface into N triangles. Triangluar mesh is picked for its versatility to construct random shape geometry.

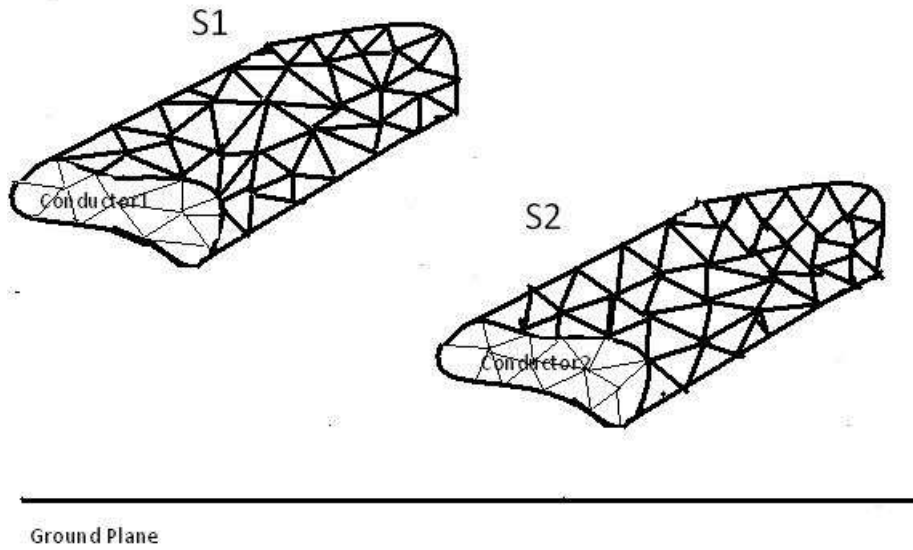


Figure 3.1: Surface triangular mesh

2. Expand unknown surface charge density into N known basis function $s_n(r)$.

$$\rho_s(\vec{r}) = \sum_{n=1}^N a_n s_n(\vec{r}) \quad (3.1)$$

with unknown coefficients a_n and pulse basis function $s_n(\vec{r})$ which is equal to one for triangle n and equals zero for all other triangles of the surface. In other words, we consider a piecewise-constant charge distribution with unknown coefficients - the staircase distribution. And average charge distribution is assumed for every triangle.

The first step of MoM is to substitute expansion Eq.(3.1) into Eq.(2.34) and interchange summation and integration. This gives

$$\varphi_{spec}(\vec{r}) = \sum_{n=1}^N \int \frac{S_n(\vec{r}')}{4\pi\epsilon_0 |\vec{r} - \vec{r}'|} dS' \quad (3.2)$$

φ_{spec} denotes the electrostatic potential, the integration variable \vec{r}' , in Eq.(3.2) belongs to surface $S = S_1 + S_2 + \dots + S_N$, whereas the observation variable \vec{r} , belongs to the same surface too. To obtain this system, we additionally multiply both sides of Eq.(3.2) by every basis function $s_1(\vec{r}), s_2(\vec{r}), \dots, s_N(\vec{r})$, and then integrate the resulting expression one more time over the surface S . These steps give Eq.(3.3)

$$\begin{aligned}
V &= \int_S \varphi_{spec}(\vec{r}') s_1(\vec{r}') dS \\
&= \sum_{n=1}^N a_n \left\{ \int_S \int_S \left(\frac{1}{4\pi\epsilon_0} \frac{s_1(\vec{r}') s_n(\vec{r}'')}{|\vec{r}' - \vec{r}''|} \right) dS' dS'' \right\} = \sum_{n=1}^N a_n Z_{1n} \quad (3.3)
\end{aligned}$$

One can see that Eq. 3.3 could be compactly written in the form of a system of linear equations:

$$\begin{aligned}
\begin{bmatrix} V_1 \\ V_2 \\ \dots \\ V_N \end{bmatrix} &= \begin{bmatrix} Z_{11} & Z_{12} & \dots & Z_{1N} \\ Z_{21} & \dots & \dots & Z_{2N} \\ \dots & \dots & \dots & \dots \\ Z_{N1} & Z_{N2} & \dots & Z_{NN} \end{bmatrix} \cdot \begin{bmatrix} a_1 \\ a_2 \\ \dots \\ a_N \end{bmatrix} \\
Z_{MN} &= \frac{1}{4\pi\epsilon_0} \int_{S_m} \int_{S_n} \frac{s_m(\vec{r}') s_n(\vec{r}'')}{|\vec{r}' - \vec{r}''|} dS' dS'' \quad (3.4) \\
V_m &= \int_{S_m} \varphi_m(\vec{r}') s_m(\vec{r}') dS
\end{aligned}$$

This is the MoM matrix for 3D metal structure for unknown coefficients a_n and at times symmetric matrix Z is the MoM matrix. Thus, the MoM method solves the system of linear equations Eq.(3.4).

3D application can be easily converted to 2D electrostatic model. As presented previously, for a transmission line, since charge is uniformly distributed along the line, only one cross-section of the line is usually of interest, which is perpendicular to the z -axis. The field and charge distribution remains the same for any cross-section. The surface integral in Eq.(2.34) over the metal surface $S = S_1 + S_2 + \dots + S_N$ will become the edge integral over the contour $l = l_1 + l_2 + \dots + l_N$ covering the cross section of all the conductors in the system. We know, from electrostatics, that any line with a charge uniformly distributed along the line will create the electric potential

$$\varphi(\vec{r}') = -\frac{\rho_l l n}{2\pi\epsilon_0} \ln |\vec{r}' - \vec{r}''| \quad (3.5)$$

where ρ_l is the charge density per unit length. Then, integral given by Eq.(2.34) is reduced to a contour integral

$$\varphi_{spec}(\vec{r}) = - \int_l \frac{\rho_l(\vec{r}') \ln |\vec{r} - \vec{r}'|}{2\pi\epsilon_0} dl' \quad (3.6)$$

For 2D problem, edge basis function is used. The entire contour l is divided into N small straight segments (edges) and unknown charge density ρ_l is expanded into N known basis functions $s_n(\vec{r})$. Then, following the same steps for 3D geometry, we will acquire the results as:

$$\begin{aligned} \begin{bmatrix} V_1 \\ V_2 \\ \dots \\ V_N \end{bmatrix} &= \begin{bmatrix} Z_{11} & Z_{12} & \dots & Z_{1N} \\ Z_{21} & \dots & \dots & Z_{2N} \\ \dots & \dots & \dots & \dots \\ Z_{N1} & Z_{N2} & \dots & Z_{NN} \end{bmatrix} \cdot \begin{bmatrix} a_1 \\ a_2 \\ \dots \\ a_N \end{bmatrix} \\ Z_{MN} &= \frac{1}{2\pi\epsilon_0} \int_l \int_l s_m(\vec{r}) s_n(\vec{r}') \ln |\vec{r} - \vec{r}'| dl' dl \\ V_m &= \int_l \varphi_{spec}(\vec{r}) s_m(\vec{r}) dl \end{aligned} \quad (3.7)$$

As introduced previously, the present MoM method is called the Galerkin method; it uses the special testing procedure (second integration) plus the same basis and testing functions. In another, simpler MoM formulation (collocation or point matching), we just pick up N discrete versions of Eq.(3.6), say, for every edge midpoint and thus arrive at another complete system of N MoM equations, which may be very similar to the present one.

3.2.2 Integral calculation

The elements of the MoM matrix are expressed in the form of double integrals; those integrals should be evaluated either numerically or analytically. As explained in Sec.3.1, we use the simplest midpoint numerical integration.

1. For 3D geometry, in Eq.(3.4), when $m \neq n$, the simplest midpoint numerical integration can be used to solve the non-singular terms in MoM matrix, it gives

$$Z_{mn} \cong \frac{A_m A_n}{4\pi\epsilon_0 |\vec{c}_m - \vec{c}_n|}, V_m \cong A_m \varphi_{spec}(\vec{c}_m) \quad (3.8)$$

where A_i, \vec{c}_i are triangle area and center of the triangle, respectively. The approximation given by Eq.(3.8) fails when $m = n$. In this case, we use the analytical integration[16] presents analytical formulas for MoM self-coupling terms involving the scalar Green function of free space. It can be used for near-field calculations of electric and magnetic source currents, especially for the calculation of method of moments (MoM) matrix elements due to the solution of surface integral equations.

The singular contributions of all necessary integrals can be reduced to

$$\begin{aligned} & \int \int_{S'} \frac{1}{|\vec{r} - \vec{r}'|} dS', \quad \int \int_{S'} \lambda' \frac{1}{|\vec{r} - \vec{r}'|} dS' \\ & \int \int_{S'} \lambda' \nabla \frac{1}{|\vec{r} - \vec{r}'|} dS', \quad \int \int_{S'} \nabla \frac{1}{|\vec{r} - \vec{r}'|} dS' \end{aligned} \quad (3.9)$$

where λ_j are the simplex coordinates or normalized area coordinates on the source triangle. Since the singular contributions of all necessary integrals can be reduced to

$$\begin{aligned} Z_{mm} &= \int_S \int_S \left(\frac{1}{4\pi\epsilon_0} \frac{s_m(\vec{r}) s_m(\vec{r}')}{|\vec{r} - \vec{r}'|} \right) dS' dS \\ &= \frac{1}{4\pi\epsilon_0} \int \int_S \frac{1}{|\vec{r} - \vec{r}'|} dS' dS \end{aligned} \quad (3.10)$$

we only consider the singular self-coupling terms of Eq.(3.10) for arbitrary linear source distributions on the triangle

$$I = \frac{1}{4A^2} \int \int_S \int \int_S \frac{1}{|\vec{r} - \vec{r}'|} dS' dS \quad (3.11)$$

Because we consider self-coupling terms, we can write

$$\vec{r} = \lambda_1(\vec{r}_1 - \vec{r}_2) + \lambda_2(\vec{r}_2 - \vec{r}_3) + \vec{r}_3, \quad \vec{r}' = \lambda'_1(\vec{r}_1 - \vec{r}_3) + \lambda'_2(\vec{r}_2 - \vec{r}_3) + \vec{r}_3 \quad (3.12)$$

Therefore:

$$\vec{r} - \vec{r}' = (\lambda_1 - \lambda'_1)(\vec{r}_1 - \vec{r}_3) + (\lambda_2 - \lambda'_2)(\vec{r}_2 - \vec{r}_3) \quad (3.13)$$

The \vec{r}_i are the corners of the triangle. Integral over the triangle area can be easily

solved with the coordinate transformation. Then we get:

$$\begin{aligned}
I &= \frac{\log\left(\frac{(a-b+\sqrt{a}\sqrt{a-2b+c})(b+\sqrt{a}\sqrt{c})}{(-b+\sqrt{a}\sqrt{c})(-a+b+\sqrt{a}\sqrt{a-2b+c})}\right)}{6\sqrt{a}} + \\
&+ \frac{\log\left(\frac{(-b+c+\sqrt{c}\sqrt{a-2b+c})(b+\sqrt{a}\sqrt{c})}{(-b+\sqrt{a}\sqrt{c})(b-c+\sqrt{c}\sqrt{a-2b+c})}\right)}{6\sqrt{c}} \\
&+ \frac{\log\left(\frac{(a-b+\sqrt{a}\sqrt{a-2b+c})(-b+c+\sqrt{c}\sqrt{a-2b+c})}{(b-c+\sqrt{c}\sqrt{a-2b+c})(-a+b+\sqrt{a}\sqrt{a-2b+c})}\right)}{6\sqrt{a-2b+c}}
\end{aligned} \tag{3.14}$$

with $a = (\vec{r}_3 - \vec{r}_1) \cdot (\vec{r}_3 - \vec{r}_1)$, $b = (\vec{r}_3 - \vec{r}_1) \cdot (\vec{r}_3 - \vec{r}_2)$, $c = (\vec{r}_3 - \vec{r}_2) \cdot (\vec{r}_3 - \vec{r}_2)$

Thus the solution to the MoM matrix is

$$\begin{aligned}
Z_{mm} &= \int_S \int_S \left(\frac{1}{4\pi\epsilon_0} \frac{s_m(\vec{r}') s_m(\vec{r}'')}{|\vec{r}' - \vec{r}''|} \right) dS' dS'' \\
&= \frac{A_m^2}{\pi\epsilon_0} \cdot \frac{1}{4A_m^2} \int_S \int_S \frac{1}{|\vec{r}' - \vec{r}''|} dS' dS'' = \frac{A_m^2}{\pi\epsilon_0} \cdot I
\end{aligned} \tag{3.15}$$

2. For 2D geometry, apply mid-point integral to Eq.(3.7), we get

$$Z_{mn} = -\frac{h_m h_n \ln |\vec{c}_m - \vec{c}_n|}{2\pi\epsilon_0}, V_m \cong h_m \varphi_{spec}(\vec{c}_m) \tag{3.16}$$

where h_n, \vec{c}_n are edge length and midpoint edge position, respectively. Note that Eq.(3.16) predicts that our MoM matrix will be identical with that for the point matching, to within edge length multiplication. The multiplication by h_m in Eq.(3.16) may be omitted for both Z_{mn}, V_m .

Similar to case 1, the approximation given by Eq.(3.16) fails when $m = n$. In this case, we still use the analytical integration. Without loss of generality we assume that an edge under test is located along the x-axis, starting with $x = 0$. This gives

$$Z_{mm} = \frac{1}{2\pi\epsilon_0} \int_0^{h_m} \int_0^{h_m} \ln |\vec{r}' - \vec{r}''| dx' dx'' = -\frac{h_m^2 (\ln(h_m) - 1.5)}{2\pi\epsilon_0} \tag{3.17}$$

if we use integration by parts. The accuracy of self-term calculations is critical for the MoM method when the number of unknowns (edges) is small. For a large number of unknowns, the importance of self-terms diminishes.

3.2.3 Charge Conservation Law

As presented in 2.4, the elements of the capacitance matrix can easily be determined once a relationship has been established between the charge density of the conductors and the potential of the conductors.

It is customary to choose the potential of the reference conductor (ground plane) being equal to zero. All other conductors may have different nonzero potentials. Another problem that need to be considered is the charge conservation equation which states the condition of total charge being equal to zero is not explicitly imposed into the above MoM equation set. Also this is not present in some textbooks [19]. However, a simple numerical experiment with a transmission line having two non-equal conductors will show that this condition will fail, even though such an effect may initially have no visible influence on the static capacitance obtained by the MoM method - see below. In case of two equal conductors, or for a conductor above an infinite ground plane calculated by the method of images, the condition of zero net charge will be indeed satisfied automatically.

In order to satisfy this condition in every case, we will use the approach suggested in Ref. [6]. Namely, we divide each of Eq.(3.7) by the corresponding surface area (in 2D case, it's edge length), then subtract the last row of Eq.(3.7) (which corresponds to the last segment on the reference conductor) from the others, and finally replace this last equation by the charge conservation law, in the form

$$\begin{bmatrix} V_1 \\ V_2 \\ \dots \\ 0 \end{bmatrix} = \begin{bmatrix} Z_{11} & Z_{12} & \dots & Z_{1N} \\ Z_{21} & \dots & \dots & Z_{2N} \\ \dots & \dots & \dots & \dots \\ h_1 & h_2 & \dots & h_N \end{bmatrix} \cdot \begin{bmatrix} a_1 \\ a_2 \\ \dots \\ a_N \end{bmatrix} \quad (3.18)$$

3.3 MoM approach to conductor with dielectric layer

After an initial excitement about the simple static MoM application for metal conductors, a more difficult and realistic application is to include the dielectric into consideration. The method described below will follow classic references [66, 56, 43].

While the metal conductors have only free surface density , on metal surfaces, in the presence of dielectric, the conditions is complicated for the existence of polarized charge on metal-dielectric interface and dielectric-dielectric interface and thus possesses an extra bound surface charge density. In this section, an integral representation of the Green's functions for the desired mathematical model is presented in which ground planes are assumed at finite distances from the dielectric sheet. However, in chapter4 final results are obtained only for the case in which ground planes are at infinity.

Modeling multi-conductor transmission lines in a multilayered board is different from modeling multi-conductor transmission lines embedded in multilayered board. Thus, different conditions need to be discussed separately in this section.

3.3.1 Poisson's equation

The dielectric can possess the bound surface charge density but does not have the volume polarization currents since the problem is static in nature. Therefore, according to equivalence principle, the dielectric material could be removed and replaced by those charges. The Poisson's equation Eq.(2.31) remains the same, with the exception of the fact that instead of the free charge density on metal surface one should consider the total charge density either on metal-dielectric surface or on a dielectric-dielectric interface. The electric potential is now caused by total charges on metal-dielectric and dielectric-dielectric interfaces. One thus has [64, 56, 6]

$$\Delta\varphi_{spec} = -\frac{\rho_{total}}{\epsilon_0} \quad (3.19)$$

where ρ_{total} is the total surface (or line) charge density on an interface. Note that Eq.(3.19) is indeed reduced to the classic result[19]

$$\Delta\varphi_{spec} = -\frac{\rho_f}{\epsilon_0\epsilon_r} \quad (3.20)$$

if we replace the total charge density by free charge density on the metal-dielectric surface,

$$\Delta\varphi_{spec} = -\frac{\rho_f}{\epsilon_r} \quad (3.21)$$

Except the change for charge density, $\varphi_{spec}(\vec{r})$ in above equation is again given on metal conductors but not on the dielectric-dielectric interfaces. Other variables are explained in above section. We therefore need to extend the present formulation by the corresponding boundary conditions at metal-dielectric interface and dielectric-dielectric interface.

The normal component of an electric displacement \vec{D} ,

$$\vec{D} = \epsilon_0 \epsilon_r \vec{E} \quad (3.22)$$

must be continuous at a dielectric-dielectric interface. This is an extra boundary condition that is used to complete the system of MoM equations as explained in Chapter 2.

3.3.2 Multi-conductor transmission line in a multilayered dielectric region above infinity ground plane

Consider a system of multiconductor transmission lines in a multilayered dielectric region above a ground plane with the uppermost dielectric extends to $y = +\infty$ or an upper ground plane. An arbitrary number N_c of perfect conductors are embedded in an arbitrary number N_d of dielectric layers. Let's say the permittivity of the j th dielectric layer is ϵ_j . A lower ground plane extended from $x = -\infty$ to $x = +\infty$ is present. (In the first case, the brick geometry is with an infinite-ground plane) Nominally, the upper ground plane and the dielectric layers also extend from $x = -\infty$ to $x = +\infty$ which will be truncated at a finite value in the numerical analysis similar to the first case.

A total charge ρ_T is assumed on the conductor-to-dielectric interfaces and the $N_d - 1$ dielectric-to-dielectric interfaces. The conductor-to-dielectric interfaces consist of the surface of the N_c conductors and the upper ground plane, if present. The j th dielectric-to-dielectric interface is defined as the plane of constant y where the dielectric layers ϵ_j and ϵ_{j+1} meet. In the other case, if conductors lie on this plane, then the j th dielectric-to-dielectric interface is the portion of this plane not occupied by conductors.

Here, we started to analyze this system with the first case- the uppermost dielectric extends to $y = +\infty$. At any point \vec{r} in the xy plane and above the lower ground plane. The potential φ_{spec} is due to the combination of ρ_T and the image of ρ_T about the lower

ground plane. Hence with Eq.(3.6), we get

$$\varphi_{spec}(\vec{r}) = \frac{1}{4\pi\epsilon_0} \sum_{j=1}^J \int_{S_j} \rho_T(\vec{r}') \left(\frac{1}{|\vec{r} - \vec{r}'|} - \frac{1}{|\vec{r} - \hat{\vec{r}}'|} \right) dS' \quad (3.23)$$

where S_j is the surface area of the j th interface, dS' is the differential element of area at r' on S_j and $\hat{\vec{r}}'$ is the image of \vec{r}' about the lower ground plane. Accordingly

$$J = J_1 + J_2 \quad (3.24)$$

where $J_1 = N_c$, $J_2 = N_d - 1$.

Since the electric field is given in Chapter2 as $\vec{E}(\vec{r}) = -\nabla\varphi(\vec{r})$. Substituteing it for φ_{spec} in Eq.(3.23), and assuming that \vec{r} is not on any of the interfaces $\{S_j\}$ so that the ∇ operator may be taken under the integra sign, we obtain:

$$\vec{E}(\vec{r}) = \frac{1}{4\pi\epsilon_0} \sum_{j=1}^J \int_{S_j} \rho_T(\vec{r}') \left[\frac{\vec{r} - \vec{r}'}{|\vec{r} - \vec{r}'|^3} - \frac{\vec{r} - \hat{\vec{r}}'}{|\vec{r} - \hat{\vec{r}}'|^3} \right] dS' \quad (3.25)$$

Taking the limit of Eq.(3.25) as \vec{r} approaches the interface S_j at \vec{r} . We obtain the following formula for $\vec{E}(\vec{r})$ valid on S_j :

$$\vec{E}^{\pm}(\vec{r}) = \frac{1}{4\pi\epsilon_0} \sum_{j=1}^J \int_{S_j} \rho_T(\vec{r}') \left[\frac{\vec{r} - \vec{r}'}{|\vec{r} - \vec{r}'|^3} - \frac{\vec{r} - \hat{\vec{r}}'}{|\vec{r} - \hat{\vec{r}}'|^3} \right] dS' \pm \vec{n} \frac{\rho_T(\vec{r}')}{2\epsilon_0} \quad (3.26)$$

where \vec{r} on S_i $i = 1, 2, \dots, J$, \vec{n} is the unit vector normal to S_j at \vec{r} .

The side of S_j toward which \vec{n} points is called the positive side of S_j corresponding to \vec{E}^+ in Eq(3.26) while the side of S_j away from which \vec{n} points is called the negative side of S_j corresponding to \vec{E}^- , in Eq(3.26), \int_{S_j} denotes principal value of the integral over S_j .

On each conductor-to-dielectric interface, the potential is constant. Denoting the potential on the i th conductor-to-dielectric interface by V_i we obtain

$$\varphi_{spec}(\vec{r}) = V_i \quad (3.27)$$

where r_i is on S_i , $i = 1, 2, \dots, J_1$.

Then subsitution of Eq.(3.27) for $\varphi_{spec}(\vec{r})$ in Eq.(3.23) yields

$$\frac{1}{4\pi\epsilon_0} \sum_{j=1}^J \int_{S_j} \rho_T(\vec{r}') \left(\frac{1}{|\vec{r} - \vec{r}'|} - \frac{1}{|\vec{r} - \vec{r}'|} \right) dS' = V_i \quad (3.28)$$

where r_i is on S_i , $i = 1, 2, \dots, J_1$.

For dielectric-to-dielectric surface, boundary condition shown in Eq(3.23) needed to be considered. Under such condition, we got:

$$\epsilon_{i-J_1} E^+(\vec{r}) \cdot \vec{n} = \epsilon_{i+1-J_1} E^-(\vec{r}) \cdot \vec{n} \quad (3.29)$$

where \vec{r} on S_i $i = J_1 + 1, J_2 + 2, \dots, J$

In Eq(3.29), ϵ_{i-J_1} and $E^+(\vec{r})$ are, respectively, the permittivity and electric field on the upper side of S_j . Moreover, ϵ_{i+1-J_1} and $E^-(\vec{r})$ are respectively the permittivity and electric field on the lower side of S_j . Substitution of Eq(3.26) for $\vec{E}^\pm(\vec{r})$ in Eq(3.29), after divided by $(\epsilon_{i-J_1} - \epsilon_{i+1-J_1})$

$$\begin{aligned} & \frac{(\epsilon_{i-J_1} + \epsilon_{i+1-J_1})}{2\epsilon_0(\epsilon_{i-J_1} - \epsilon_{i+1-J_1})} \rho_T(\vec{r}) + \\ & \frac{1}{4\pi\epsilon_0} \sum_{j=1}^J \int_{S_j} \rho_T(\vec{r}') \left[\frac{\vec{r} - \vec{r}'}{|\vec{r} - \vec{r}'|^3} - \frac{\vec{r} - \vec{r}'}{|\vec{r} - \vec{r}'|^3} \right] \cdot \vec{n} dS' = 0 \end{aligned} \quad (3.30)$$

\vec{r} on S_i $i = J_1 + 1, J_2 + 2, \dots, J$

Eq.(3.28) and Eq.(3.30) are a set of J integral equations in the unknown total charge ρ_T on the interfaces whose patches are $(S_j, j = 1, 2, \dots, J)$

There are special conditions when some of the conductors may be of finite cross section, and others may be infinitely thin strip. The boundary condition can be simplified for those conditions. Regardless of this, the free charge Q per unit length on the conductor is given by[56]

$$Q_i = \int_{S_i} \rho_F(\vec{r}) dS, \quad i = 1, 2, \dots, N_c \quad (3.31)$$

where dS is the differential element of length at \vec{r} on S_i . Development of the Moment solution based on current model. In this section, the integral equations (3.28) and (3.30) are solved numerically for ρ_T by means of the method of moments. A solution ρ_T to Eq(3.28)

and (3.30) is sought in the form

$$\rho_T(\vec{r}) = \sum_{n=1}^N \rho_{Tn} s_n(\vec{r}) \quad (3.32)$$

where $\{s_n(\vec{r}), n = 1, 2, \dots, N\}$ are unit pulse functions which cover $\{S_j, j = 1, 2, \dots, J\}$ and σ_{Tn} is the unknown coefficients.

$$\begin{aligned} V_1 &= \int_S \varphi_{spec}(\vec{r}) s_1(\vec{r}) dS \\ &= \sum_{n=1}^N \rho_{Tn} \left\{ \int_S \int_S \frac{1}{4\pi\epsilon_0} \left(\frac{1}{|\vec{r} - \vec{r}^j|} - \frac{1}{|\vec{r} - \vec{r}^j|} \right) dS' dS \right\} = \sum_{n=1}^N \rho_{Tn} Z_{1n} \\ V_1 &= \int_S \varphi_{spec}(\vec{r}) s_1(\vec{r}) dS \\ &= \sum_{n=1}^N \rho_{Tn} \left\{ \int_S \int_S \frac{1}{4\pi\epsilon_0} \left(\frac{1}{|\vec{r} - \vec{r}^j|} - \frac{1}{|\vec{r} - \vec{r}^j|} \right) dS' dS \right\} = \sum_{n=1}^N \rho_{Tn} Z_{1n} \\ \dots & \\ V_{N_1} &= \int_S \varphi_{spec}(\vec{r}) s_{N_1}(\vec{r}) dS \\ &= \sum_{n=1}^N \rho_{Tn} \left\{ \int_S \int_S \frac{1}{4\pi\epsilon_0} \left(\frac{1}{|\vec{r} - \vec{r}^j|} - \frac{1}{|\vec{r} - \vec{r}^j|} \right) dS' dS \right\} \quad (3.33) \\ &= \sum_{n=1}^N \rho_{Tn} Z_{N_1 n} \\ \dots \dots \dots & \\ 0 &= \sum \rho_{Tn} \left\{ \int_S \int_S \left(\frac{1}{4\pi\epsilon_0} \left(\frac{|\vec{r} - \vec{r}^j|}{|\vec{r} - \vec{r}^j|^3} - \frac{|\vec{r} - \vec{r}^j|}{|\vec{r} - \vec{r}^j|^3} \right) \cdot \vec{n} \right) dS' dS \right\} \\ &+ \sum \rho_{Tn} \left\{ \frac{(\epsilon_{i-J_1} - \epsilon_{i+1-J_1})}{2\epsilon_0(\epsilon_{i-J_1} - \epsilon_{i+1-J_1})} \right\} = \sum_{n=1}^N \rho_{Tn} Z_{N_1+1n} \\ \dots & \\ 0 &= \sum \rho_{Tn} \left\{ \int_S \int_S \left(\frac{1}{4\pi\epsilon_0} \left(\frac{|\vec{r} - \vec{r}^j|}{|\vec{r} - \vec{r}^j|^3} - \frac{|\vec{r} - \vec{r}^j|}{|\vec{r} - \vec{r}^j|^3} \right) \cdot \vec{n} \right) dS' dS \right\} \\ &+ \sum \rho_{Tn} \left\{ \frac{(\epsilon_{i-J_1} - \epsilon_{i+1-J_1})}{2\epsilon_0(\epsilon_{i-J_1} - \epsilon_{i+1-J_1})} \right\} = \sum_{n=1}^N \rho_{Tn} Z_{Nn} \end{aligned}$$

Now let $\{s_n(\vec{r}), n = 1, 2, \dots, N_1\}$ be the pulse on $\{S_j, j = 1, 2, \dots, J_1\}$ and let $\{s_n(\vec{r}), n = N_1 + 1, N_1 + 2, \dots, N\}$ be the pulse on $\{S_j, j = J_1 + 1, J_1 + 2, \dots, J\}$. Sub-

stituting Eq.(3.32) for ρ_T in Eq.(3.28) and Eq.(3.30), then interchange summation and integration. Then, we will follow the Galerkin method stated in Sec.3.2.1. We thus multiply both sides of Eq.(3.28) and (3.30) by every basis function, $s_1(\vec{r}), s_2(\vec{r}), \dots, s_N(\vec{r})$, and then integrate the resulting expression one more time over the surface S which composed by $\{S_1, S_2, \dots, S_J\}$. These steps result in the system of MoM equations in the form shown as Eq(3.33). The first part of the equation are for the metal-dielectric interface. It's the same as Eq(3.6) for metal geometry. The second part are those for dielectric-to-dielectric surface. In this paper, Metal-dielectric method is only realized for 2D problem as shown in Sec.3.3.3.

3.3.3 2D Multiconductor transmission line in a multilayered dielectric region with finite-ground plane

Consider a multi-conductor systems with a finite-ground plane. Thus in Eq(3.6), we don't need to apply the image theory to source point. Combined with Eq.(3.17) for the case with 2D Multiconductor transmission line in a multilayered dielectric region with finite-ground plane, the solution Eq. (3.28) and (3.30) will be simplified to:

$$\frac{1}{2\pi\epsilon_0} \sum_{j=1}^J \int \rho_T(\vec{r}') \ln |\vec{r} - \vec{r}'| dl' = V_i \quad (3.34)$$

$$\frac{(\epsilon_{i-J_1} + \epsilon_{i+1-J_1})}{2\epsilon_0(\epsilon_{i-J_1} - \epsilon_{i+1-J_1})} \rho_T(\vec{r}) - \frac{1}{2\pi\epsilon_0} \sum_{j=1}^J \int \rho_T(\vec{r}') \frac{|\vec{r} - \vec{r}'|}{|\vec{r} - \vec{r}'|^2} \cdot \hat{n} dl' = 0 \quad (3.35)$$

In this case, the impedance matrix for MoM also changed to

$$Z_{mn} = \int \int_l \left(\frac{1}{2\pi\epsilon_0} \ln |\vec{r} - \vec{r}'| \right) dl' dl \quad (3.36)$$

where $m = 1, 2, \dots, N_1$

$$Z_{mn} = - \int \int_l \left(\frac{1}{2\pi\epsilon_0} \cdot \frac{|\vec{r} - \vec{r}'|}{|\vec{r} - \vec{r}'|^2} \cdot \hat{n} \right) dl' dl + \frac{(\epsilon_{i-J_1} - \epsilon_{i+1-J_1})}{2\epsilon_0(\epsilon_{i-J_1} - \epsilon_{i+1-J_1})} \quad (3.37)$$

where $m = N_1 + 1, N_1 + 2, \dots, N$

The elements of the MoM matrix are again expressed in the form of double integrals; those integrals should be evaluated either numerically or analytically. For the reasons discussed yet in Section 3.1, we prefer to use the simple midpoint numerical integration. The midpoint integration gives

$$Z_{mn} \approx -\frac{h_m h_n \ln |\vec{c}_m - \vec{c}_n|}{2\pi\epsilon_0}, V_m \approx h_m \varphi_{spec}(\vec{c}_m) \quad (3.38)$$

For the elements of the impedance matrix with metal edges. Simultaneously, for the elements of the impedance matrix with the dielectric edges, one has,

$$\begin{aligned} Z_{mn} &\approx (\epsilon_{i-J_1} - \epsilon_{i+1-J_1}) \frac{h_m h_n ((\vec{c}_m - \vec{c}_n) \cdot \vec{n}_m)}{2\pi\epsilon_0 |\vec{c}_m - \vec{c}_n|^2} - \frac{(\epsilon_{i-J_1} + \epsilon_{i+1-J_1})}{2\epsilon_0} h_m \\ V_m &\approx h_m \varphi_{spec}(\vec{c}_m) \end{aligned} \quad (3.39)$$

where h_n, \vec{c}_n are edge length and the midpoint edge position, respectively.

The approximation given by Eq.(3.38) and Eq.(3.39) again fails when $m = n$. In this case, we use the analytical integration which gives Eq.(3.40) and (3.41). For the metal edges

$$Z_{nn} = -\int_0^{h_n} \int_0^{h_n} \frac{\ln |x - x'|}{2\pi\epsilon_0} dx dx' = -\frac{h_n^2 (\ln(h_n) - 1.5)}{2\pi\epsilon_0} \quad (3.40)$$

If we use integration by parts. The accuracy of self-term calculations is critical for the MoM method when the number of unknowns (edges) is small. For the dielectric self-terms, the term with the unit normal will give exactly zero, due to zero dot product, so that one simply has

$$z_{nn} \approx -\frac{(\epsilon_{i-J_1} - \epsilon_{i+1-J_1})}{2\epsilon_0} h_n \quad (3.41)$$

3.4 Conclusion

It has been demonstrated in this paper that the static charge distribution on a charged conductor of arbitrary shape can be numerically determined by a method of moments approach. In the approach used here, the surface of the conductor is approximated by planar triangular patches. In contrast to other patch shapes, they have the advantages

of simplicity, generality, and of complete flexibility in their placement. In the model used here the charge is assumed to be constant within each planar triangle region, yielding a piecewise constant or pulse representation of the charge on the conducting surface. The integral Eq.(3.23) and (3.26) for the total charge at the surfaces of conductors embedded in multiple dielectric, regions and on the dielectric-to-dielectric interfaces are simple in concept. The singular kernels considered is the 3-D Green's function for the static case. The solution obtained by the method of moments is also simple shown as Eq.(3.33). Numerical results in Chapter4 shows that this type of solution is both versatile and accurate. Improvement in the rate of convergence can be obtained by using adaptive refinement, but at the cost of considerable complication.

Chapter 4

MATLAB Implementation and Numerical results

Aiming at calculating the capacitance matrix for the transmission line and interconnect structures involving multiple layers of irregularly shaped conductors imbedded in different dielectric materials, MATLAB was used to implement the 2D MoM Metal-Dielectric Algorithm and 3D Metal algorithm. Computed numerical results are compared to analytical results as well as results from commercial software, such as Ansoft HFSS, Field Precision Package.

4.1 GUI Design with MATLAB

To realize the MoM in MATLAB, we designed a friendly interface called MoMtool to integrate the function introduced in Chapter 3. Fig.(4.1) is the MainMenu for MoM tool including 2D/3D mesh generation, 2D/3D capacitance extraction solver and Mesh/Charge reviewer.

As shown in Fig.(4.2), triangular mesh is picked in MoM tool and the common way of doing this originated from old NASTRAN program written in late 1960s. It is demonstrated by Eq.(4.1). First, we create a $3 \times N$ array of 3D (or 2D) nodes, P . Next, we create a $4 \times M$ array of triangle vertexes, t . Each vertex is an index into the array of nodes. The last row

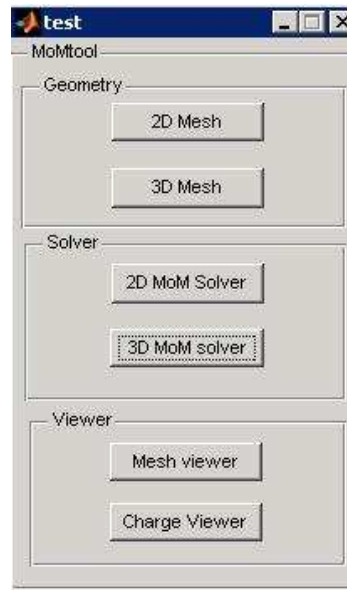


Figure 4.1: MainMenu

Planar mesh generator based on delaunay2
All units are millimeters

Rectangles & Ellipses

Region	Name	xc	yc	Shape	Width	Height	Border	Border width
S1	DummyDee	x_shift	y_shift+th/2	<input checked="" type="checkbox"/> <input type="checkbox"/>	W	th	<input type="checkbox"/>	
S2	RfDee	x_shift	-y_shift-th/2	<input checked="" type="checkbox"/> <input type="checkbox"/>	W	th	<input type="checkbox"/>	
S3	RfDee2	x_shift	0	<input checked="" type="checkbox"/> <input type="checkbox"/>	W	th	<input type="checkbox"/>	
S4				<input checked="" type="checkbox"/> <input type="checkbox"/>			<input type="checkbox"/>	
S5				<input checked="" type="checkbox"/> <input type="checkbox"/>			<input type="checkbox"/>	
S6				<input checked="" type="checkbox"/> <input type="checkbox"/>			<input type="checkbox"/>	
S7				<input checked="" type="checkbox"/> <input type="checkbox"/>			<input type="checkbox"/>	
S8				<input checked="" type="checkbox"/> <input type="checkbox"/>			<input type="checkbox"/>	
S9				<input checked="" type="checkbox"/> <input type="checkbox"/>			<input type="checkbox"/>	
S10				<input checked="" type="checkbox"/> <input type="checkbox"/>			<input type="checkbox"/>	

Set formula:

Parameters

Name	Name	Name	Name	Name	Name	Name	Name
x_shift	y_shift	W	th				
Value(s)	Value(s)	Value(s)	Value(s)	Value(s)	Value(s)	Value(s)	Value(s)
0	20	40	2				

Triangle size

Figure 4.2: 2D Mesh Interface

Figure 4.3: 3D Mesh Interface

of array t is the domain number which indicates the domain a given triangle belong to.

$$P = \begin{bmatrix} 0.1 & 0.2 & 0.1 & & 0 \\ 0.2 & 0.3 & 0.2 & \dots & 0 \\ 0.3 & 0 & 0 & & 0.5 \end{bmatrix}$$

$$t = \begin{bmatrix} 1 & 3 & 2 & & 115 \\ 2 & 4 & 7 & & 162 \\ 3 & 5 & 9 & \dots & 138 \\ 1 & 1 & 2 & & 2 \end{bmatrix} \tag{4.1}$$

Such a way of mesh representation is straightforwardly extended to a 3D case: the array of triangles, t , is replaced by an array of tetrahedra, T , with four vertexes instead of three. MATLAB can also do a 3D mesh generation.

For 2D problems, the user can specify the primitives in terms of parameters. `struct2d.m`

in 2D solver interface shown in Fig.(4.2). GUI itself has no built-in limit on the number of values that each parameter may take on. Since 3D solver is only designed for Metal 3D structure, the simulated object used for 3D structure is defaulted as metal. The 3D mesh interface shown in Fig.(4.3) is used to construct 3D geometry based on 2D mesh.

There are two main limitations of the MoMtool.

1. The user is limited to ten differently-shaped primitives, while a primitive can be cloned at different locations; clones have the same shape, dimensions, and orientation.
2. 2D solver works for metal conductors embeded in different dielectric layers while 3D solver is only designed for metal conductor system in free space without common boundary.

4.2 Matrix calculation in MATLAB

As we know from Eq.(3.1) and Eq.(3.3), two major parts in MATLAB solver of MoM is to solve impedance matrix Z and unknown coefficient matrix a . We already presented analytical solution for Z under a case in Chapter3. After the calculation of Z , a is the solution of linear Eq.(3.3) which is solved as $a = (Z \setminus V)'$ where Z is a $N \times N$ square matrix and V is a column vector with N components. In MATLAB implementation, left matrix divide ' \setminus ' is utilized.

Considering the solution to a general linear equation denoted by $X = A \setminus B$, the specific algorithm used depends upon the structure of the coefficient matrix A . To determine the structure of A and select the appropriate algorithm, MATLAB software follows this precedence[2]:

1. If A is sparse and diagonal, X is computed by dividing by the diagonal elements of A .
2. If A is sparse, square, and banded, then banded solvers are used.
3. If A is upper or lower triangular matrix, then X is computed quickly with a backsubstitution algorithm for upper triangular matrices, or a forward substitution algorithm

for lower triangular matrices. The check for triangularity is done for full matrices by testing for zero elements and for sparse matrices by accessing the sparse data structure. If A is a full matrix, computations are performed using the Basic Linear Algebra Subprograms (BLAS) routines.

4. If A is a permutation of a triangular matrix, then X is computed with a permuted backsubstitution algorithm.
5. If A is symmetric, or Hermitian, and has real positive diagonal elements, then a Cholesky factorization is attempted. If A is found to be positive definite, the Cholesky factorization attempt is successful and requires less than half the time of a general factorization. Nonpositive definite matrices are usually detected almost immediately, so this check also requires little time.
6. If A is sparse, then MATLAB software uses CHOLMOD to compute X .
7. If A is not sparse but is symmetric, and the Cholesky factorization failed, then MATLAB solves the system using a symmetric, indefinite factorization.
8. If A is Hessenberg, but not sparse, it is reduced to an upper triangular matrix and that system is solved via substitution
9. If A is square and does not satisfy criteria 1 through 6, then a general triangular factorization is computed by Gaussian elimination with partial pivoting.
10. If A is not square, then Householder reflections are used to compute an orthogonal-triangular factorization

Because of the use of charge conservation law, impedance matrix Z lost the symmetric property acquired from the double integral analytical solution. Thus Z is square and does not satisfy criteria 1 through 6, Gaussian elimination with partial pivoting will be chosen.

4.3 Mesh refinement and Convergence discussion

As stated in Chapter1, locally or adaptively refined meshes are necessary to simulate applications involving multi-scale phenomena in the geosciences. In particular, for situations

with complex geometries or domain boundaries, meshes with triangular or tetrahedral cells demonstrate their superior ability to accurately represent relevant realistic features which need complex data structure implemented[7]. In order to better account for a correct charge distribution and accurate capacitance, adaptive mesh refinement is also applied in MoMtool. To facilitate mathematical efficiency in dynamic local refinement, two distinct steps need to be considered:

1. An efficient refinement strategy leads to locally and highly dynamically refined but consistent meshes.
2. A refinement criterion needs to capture the phenomenon of interest efficiently during run-time.

After these two steps, one also needs to consider the data structures which are also the normal considerations for adaptive mesh refinement, especially for complex structure. They are needed to support the dynamic hierarchical characteristic of the mesh refinement as well as the linear data access pattern preferred by numerical computations.

In MoM, which is based on integral equations but not on the differential equations, the error at any point is directly affected by all other calculated results and the adaptive mesh refinement becomes more complicated. However, some methods have been proposed which are beyond the scope of the present basic analysis. In next two subsections, adaptive mesh refinement and corresponding convergence criterion using in MoMtool will be discussed.

4.3.1 Adaptively refined mesh

In MoMtool, there are two kinds of refinement methods for 2D and 3D problems.

For 2D case, charge distribution is on the edge. After targeted edges are picked, we subdivide every such edge into two equal sub-edges. This procedure roughly halves the highest total charges and thus makes the total charges more uniform.

For 3D metal case, the charge is distributed on the surface. Refer [7] presented a simple way as triangular bisection of a marked edge to refine the triangular mesh similar to edge-divided method. Several other methods to refine cells are commonly used, regular triangular refinement for one, which intersects triangle by bisecting each edge.

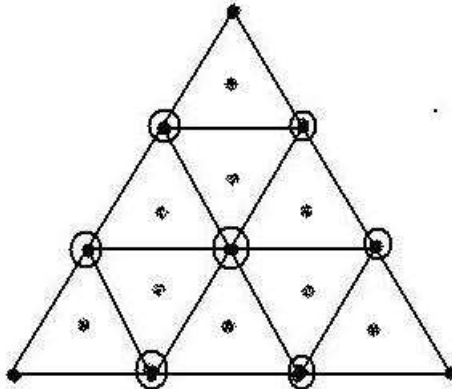


Figure 4.4: Triangle rendering using adaptive subdivision

As for MoMtool proposed in this paper, since we use mid-point integral strategy, instead of bisection, we choose triangle rendering using adaptive subdivision [34] shown in Fig.(4.4). It proved more efficient than other previous solutions and allowed the maintenance of any degree of accuracy. If a triangle is considered for refinement, the original triangle will be divided to 9 sub-triangles of equal area. Assume that the charge density of all sub-triangles is a constant, then the original integral can be written as,

$$\int_{T_m} g(\vec{r}') dS = \frac{A_m}{9} \sum_{k=1}^9 g(\vec{c}_k^c) \quad (4.2)$$

where $c_k^c (k = 1, \dots, 9)$ is the center of the 9 sub-triangles and A_m is the area of original triangle. This algorithm is extremely simple as it states that the refinement is to be repeated for all those elements that either are considered for refinement from the error estimation procedure or contain hanging nodes. In MoMtool, the algorithm terminates when the program reach demanded refinement step.

After mesh refinement, we update structure mesh and the voltage vector as shown in the script `mom2d_md.m` and `mom3d_md.m`. We then run the MoM procedure again (the solver script has a loop versus the iteration number), find the new MoM solution, calculate a new error, and make another subdivision.

An unsolved question remains: how to pick the element needed to be refined. According to Ref.[3], the goal of adaptive mesh refinement in electrostatics is to make sure that the total

charge on every sub-element stays the same. It means we need to have more basis functions (fine mesh) in the domains with large charge density and less basis functions (coarse mesh) in the domains with small charge density since these domains will perhaps hardly contribute to capacitance anyway. Based on this standard, we set up refinement criterion as follows: After the initial MoM solution is obtained, we check the total charge per edge/triangle surface given by the array field output.charge of MATLAB structure output, then we find 25% of edges/surfaces that have the highest total charge (highest areas):

$$\begin{aligned}
 charge &= abs(output.charge); \\
 [dummy, index] &= sort(charge) \\
 index &= index(round(0.75 * end) : round(1.00 * end)) \quad (4.3)
 \end{aligned}$$

The selection standard given above may have a disadvantage that elements near the corners are refined too fine, whilst other elements are virtually not refined. Since the solution is singularly close to the corners, those new elements are likely again to have maximum total charges, etc. To reduce this effect we tried to refine 25% of elements with the charge from 0% to 95% of highest instead of 25% of elements with the highest total charge. The corresponding changes are made:

$$\begin{aligned}
 charge &= abs(output.charge); \\
 [dummy, index] &= sort(charge) \\
 index &= index(round(0.70 * end) : round(0.95 * end)) \quad (4.4)
 \end{aligned}$$

However, this iteration process resulted in a failure, despite the very good convergence curve behavior. We can see it by performing a simple numerical experiment. It is suspected that one reason can be the presence of very large and very small edges as neighbors.

4.3.2 Convergence standard

To evaluate the performance of refined mesh, we need an integral quantity that will give us the criterion for the relative convergence or the relative error. Since we do not know the

exact solution, the relative convergence is the only information that we may use with regard to the solution accuracy. Usually, an energy criterion is used, for the electric and magnetic fields. An appropriate substitute in capacitance extraction may be the static capacitance itself: we define the relative error at every mesh refinement step n as

$$\Delta S = \frac{C_n - C_{n-1}}{C_n} \quad (4.5)$$

Unfortunately, Eq.(4.5) does not work well for multiconductor lines. When multiple partial capacitances exist, instead, we will use the power (or energy) criterion. One thus has Eq.(4.6) instead of Eq. (4.5),

$$\Delta S = \frac{P_n - P_{n-1}}{P_n} \quad (4.6)$$

where P_n denote energy or power. Here, the total electrostatic energy on the line or triangle surface can be easily got once we know the charge distribution following Eq.(4.7)

$$W = \frac{1}{2}CV^2 = \frac{1}{2}Re \left[\int_s V \epsilon_r \rho_{total} dS \right] \quad (4.7)$$

Thus, we can apply power convergence criterion. This criterion is implemented in the MATLAB script `mom2d_md.m` (subfolder codes) and `mom3d_md.m` (subfolder codes). We could refine the mesh multiple times. As a result, we will have a relative solution error, which is a function of the iteration number. If this function approaches to zero as the iteration number increases, the resulting solution is expected to be reasonably accurate.

One can see that error behavior is not monotonic; similar non-monotonic behavior may be also observed in the commercial software, e.g. in Ansoft HFSS. When the number of elements to be refined becomes larger, the convergence curve generally may become more smooth. Quadline model is presented in Sec.4.4.3. The convergence curve created by MoM keeps good agreement with the results we get from HFSS. Convergence figure of 3D parallel capacitor is also presented in Sec.4.5.3

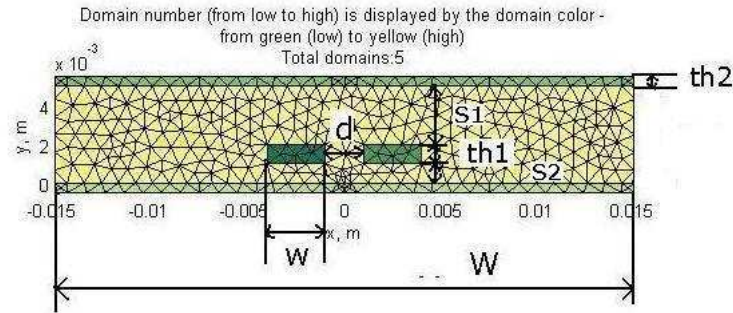


Figure 4.5: Coupled micro-strips

Table 4.1: Results comparison of coupled micro-strip line

	Ref [64]	Ref [63]	Ref [62]	MoMtool
C_{11}	9.165e-11	9.017e-11	9.224e-11	9.3343e-11
C_{12}	-8.220e-012	-8.259e-12	-8.504e-12	-8.7733e-012
C_{21}	-8.220e-012	-8.259e-12	-8.504e-12	-8.7733e-012
C_{22}	9.165e-11	9.017e-11	9.224e-11	9.3343e-11

4.4 2D Numerical examples

In this section, 2D numerical results are presented for transmission line. The result of the present analysis compared well with that available in literature as well as numerical results from commercial software package.

4.4.1 Coupled micro-strip line

Consider a pair of coupled micro-strips touching a dielectric slab over a conducting plane as shown in Fig.4.5

The left-hand conductor is conductor 1. The right-hand conductor is conductor 2. Table 4.1 compares our computed results with those of Refer[64], Refer[62] and [63]. For comparison, the results have been changed to farads per meter. For our results, we used 0.5 as triangle size and adaptive refine step setup as 10. Then a mesh with 1254 triangles and the convergence curve shows as Fig.4.5.

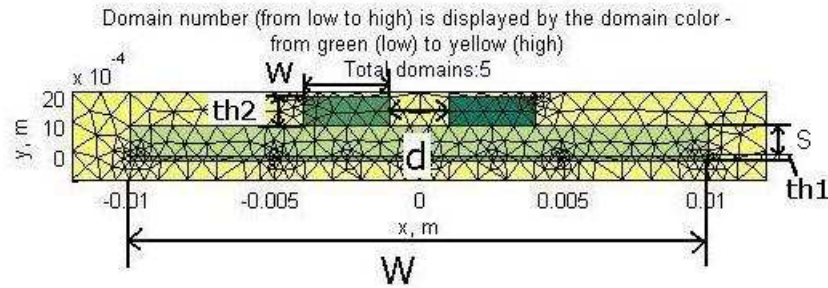


Figure 4.6: Coupled strip line

Table 4.2: Results comparison of coupled strip line

	Ref[64]	Refer[62]	MoMtool
C_{11}	6.364e-11	6.307e-11	6.3450e-11
C_{12}	-5.931e-12	-5.866e-12	-5.9069e-12
C_{21}	-5.931e-12	-5.866e-12	-5.9069e-12
C_{22}	6.364e-11	6.307e-11	6.3450e-12

4.4.2 Coupled strip line between parallel conducting planes

Fig. shows an example of coupled strip line (micro-strip line two ground planes).

The left-hand conductor is conductor 1. The right-hand conductor is conductor 2. There are two ways to build this model considering the upper ground plane. One is to truncate the upper ground plane at a finite width. Another approach is to replace the upper ground plane with a dielectric layer with much higher permittivity as discussed in [63]. MoMtool used the first method to build the model like brick structure. Simulated triangle size is 0.5 and 1440 triangles generated. Results are compared in Table4.2

4.4.3 Quadliine

A realistic example for multi-conductor transmission line would be a simple quad-transmission line used for the Dyson balun which has been widely used for standard dipoles and other symmetric antennas[42]. For the Dyson balun, it is not always convenient to use the coaxial connectors, a simple quad-transmission line vertical element can replace those coaxial cables for a turnstile while keeping the good isolation. The quad line includes a central rectangular solid metal conductor bar (copper or brass) – ground; four adjacent mi-

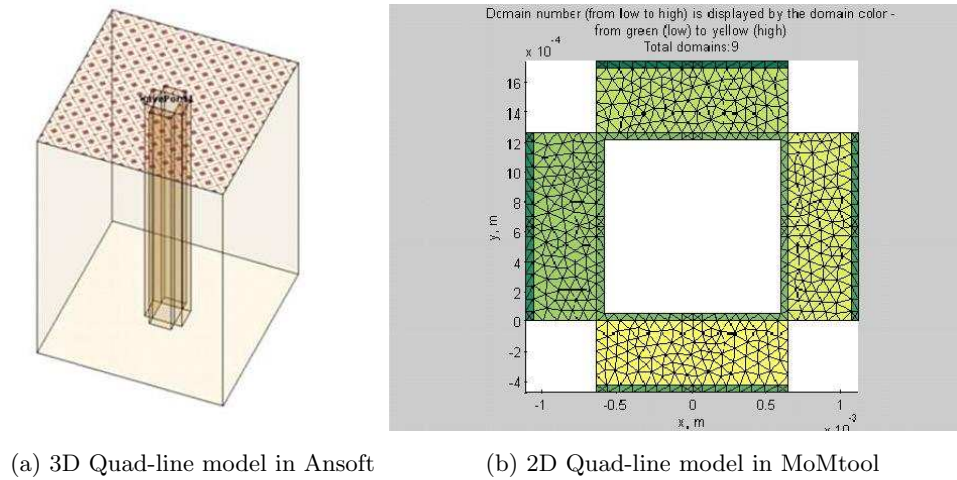


Figure 4.7: Quad-line model in Ansoft and MoMtool

crostrip transmission lines sharing the same ground. There are three steps for this example: simulation with Ansoft HFSS11, Simulation with MoM tool and comparison between these two. In Ansoft, 3D model is built shown in Fig.4.7 and the line geometry of transmission line with four signal conductors and one ground conductor is built in MoMtool shown in Fig.4.7.

The line is supposed to work as two (weakly coupled) differential lines, with two pairs of opposite conductors. As for transmission line, we first calculated its impedance with these two models. Fig.4.8 shows the error percentage of impedance between 3D model and 2D model. It's within 3 percent.

To check the effectiveness of the adaptive refinement implemented in MoMtool we made a comparison between the convergence curve of Ansoft and MoMtool under certain condition shown in Fig.4.9.

As we can see from above results, even though MoMtool employed 2D solver for transmission line model, it still keeps good accuracy. Since 2D model has much less mesh elements compared to 3D volume integral method, MoMtool is more efficient for certain models. As the final step of Quad-line simulation, we can easily get its capacitance matrix. It's given as

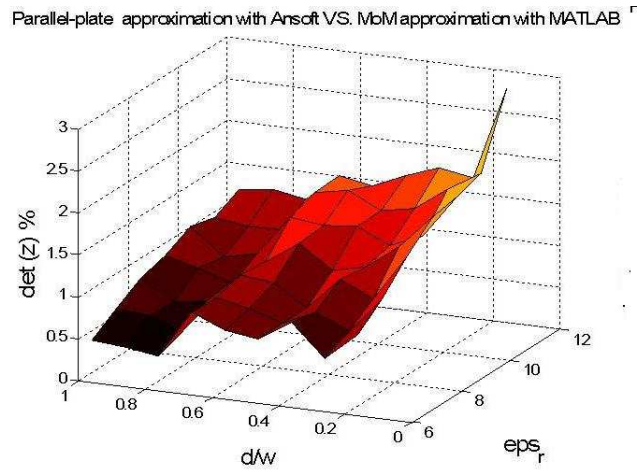
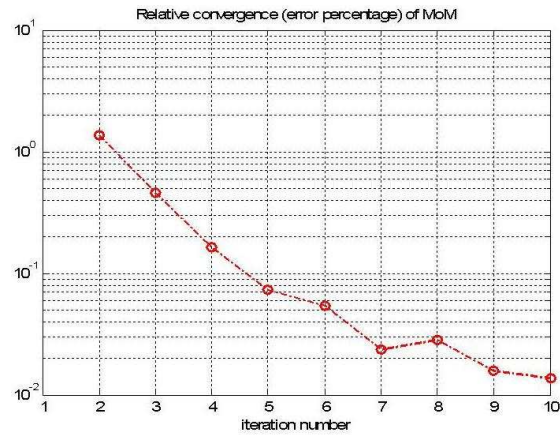
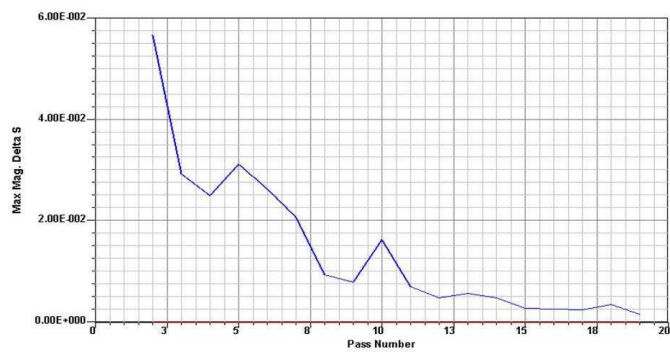


Figure 4.8: An error between Ansoft 3D results and MoMtool 2D results



(a) Convergence of Ansoft with 20 passes



(b) Convergence of MoMtool with 10 passes

Figure 4.9: Convergence comparison between Ansoft and MoMtool (eps_r=8, d/w=0.363)

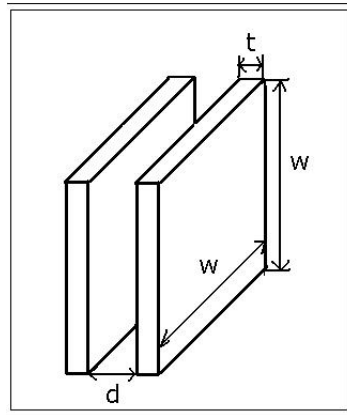


Figure 4.10: Parallel-plate square capacitor

$$C = \begin{bmatrix} 0.1802 \times 10^{-9} & -0.0067 \times 10^{-9} & -0.0067 \times 10^{-9} & -0.0010 \times 10^{-9} \\ -0.0067 \times 10^{-9} & 0.1802 \times 10^{-9} & -0.0010 \times 10^{-9} & -0.0067 \times 10^{-9} \\ -0.0067 \times 10^{-9} & -0.0010 \times 10^{-9} & 0.1802 \times 10^{-9} & 0.1802 \times 10^{-9} \\ -0.0010 \times 10^{-9} & -0.0067 \times 10^{-9} & -0.0067 \times 10^{-9} & 0.1802 \times 10^{-9} \end{bmatrix}$$

4.5 3D numerical example

To testify the effectiveness of 3D MoM stated in Chapter 3, the basic and typical example, Parallel-plate Square Capacitor is chosen. This model consists of two parallel square conductors in free space as Fig.4.10.

In basic electrostatics, the formula for the capacitance of parallel-plate capacitors is derived as Eq.(4.8) ,

$$C = \frac{\epsilon S}{d} \quad (4.8)$$

where $S = w^2$, w is the width of square plate and d is the separation between two plate. Eq.(4.8) is only for the case that the spacing between the electrodes is very small compared to the length or width of the plates and the electric charge density on the plates is uniform therefore the fringing fields at the edges can be neglected[27]. However, when the separation is wide, the formula for very small separation does not provide accurate results.

In this section, we will discuss and compare the numerical results we got from AMAZE

using Finite Element Method, refer[[45]] using Boundary Element Method and MoMtool. The simulations are done with different distance and surface area for the conductor plate. Index $b = d/w$ is used as aspect ratio to study the effect of fringe field in following sections. Larger b represents stronger influence of fringing fields.

4.5.1 AMAZE - Finite Element Method

As presented in Chapter1, finite element method has wide application in electromagnetic area. It has been used by commercial software like HFSS Ansoft. But Ansoft has limitation in finding charge solution. In this chapter, we will introduce another commercial software - AMAZE from Field Precision software package which also utilize FEM and provide full electrostatic model analysis including charge distribution.

Written by Stanley Humphries, Field Precision creates advanced finite-element software for electromagnetics. Unitized 2D and 3D packages cover a broad range of applications including electrostatics, magnet design, induction heating, charged-particle devices, permanent magnet assemblies, electromagnetic radiation, microwave devices, pulsed power systems and RF heating of biological media[1]. We utilized the following programs from the package:

MetaMesh Divides solution spaces into conformal, hexahedron elements with unique material identities to match system geometries that you specify. The output file of MetaMesh provides geometric information to the AMAZE solution programs (HiPhi, Magnum, OmniTrak, RFE3 and HeatWave) or the GamBet Monte-Carlo program.

Hiphi Calculates electrostatic fields in arbitrary three-dimensional systems. The program generates either dielectric or conductive solutions. In dielectric-type solutions, regions in the solution-space may represent electrodes, dielectrics and space-charge density. In conductive-type solutions, the regions correspond to electrodes or resistive media.

Phiview Generates plots and calculates field quantities from HiPhi solution files. It is capable of full numerical-analysis of specified field solution from Hiphi. With

regards to charge analyze function, it can be used to compute the volume of regions by taking Gaussian 12 integrals over individual hexahedron elements and give the energy and charge distribution. Also, it provides the surface integral values in response to the commanded region.

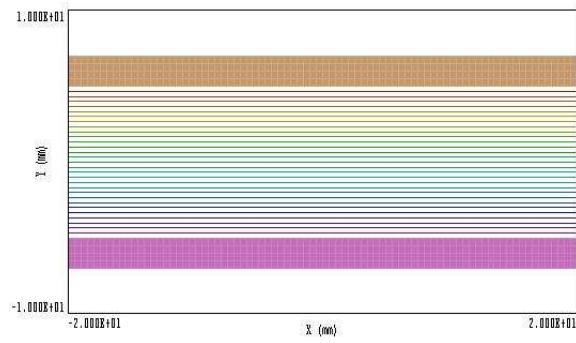
HiPhi has several advanced technical capabilities[1], but when FEM is applied open boundary problems[20]including planer transmission lines and circuits based on them, antennas, scatterers and so on, the boundary walls must be placed to limit the size of the problem domain without affecting its characteristics. Two approaches are available to deal with this. One of the commonly used approaches is to apply perfectly matched layer(PML) or analytical absorbing boundary conditions (ABC) at the walls of the device. Analysis of planar lines using this hybrid approach has been reported [13]. Another approach - conformal transformation has been employed frequently to determine the characteristics of transmission lines, and discontinuities in them. The advantage of this approach is that the analytical solution based on conformal transformation leads to design equations. An open geometry like that of planar lines is transformed into a closed geometry. The limitation of this method is that it provides solution for the static fields only [20].

However, in AMAZE boundary points have a fixed potential that is not affected by the potential at neighboring nodes. For electrostatic problems, node potentials on the boundary can be set to one of two conditions[1],

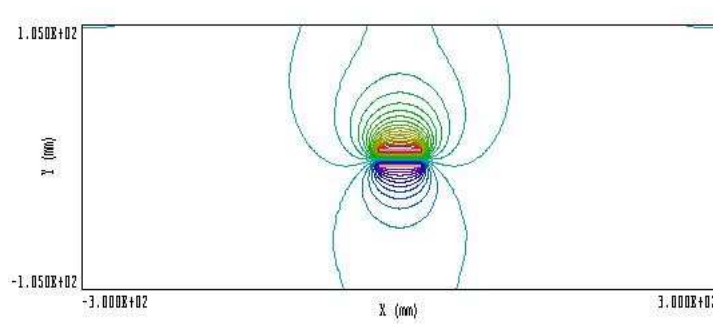
- Dirichlet condition where the electric field lines are normal to such a surface.
- Neumann condition where the electric field is parallel to the boundary.

Since in MoMtool, the parallel-plate square capacitor is treated as open boundary problem, we need to set up FEM model in the same way for the comparison purpose. As we discussed above, the charge distribution on the surface of two parallel plates is not uniform considering the fringe-effect which is shown in Fig.4.10. Thus, the first problem we need to solve is the optimized size of boundary box so that the simulation results from FEM full presented fringe-effect without being influenced by boundary condition.

Simulation is done with boundary box with different size in ratio to the size of capacitor which here is $w = 40mm$, $d = 10mm$, $th = 2mm$. Fig.4.12 shows the simulation results.



(a) Boundary box 40mm X 20mm X 40mm



(b) Boundary box 600mm X 105mm X 600mm

Figure 4.11: Electric field of Parallel-plate Square Capacitor in FEM

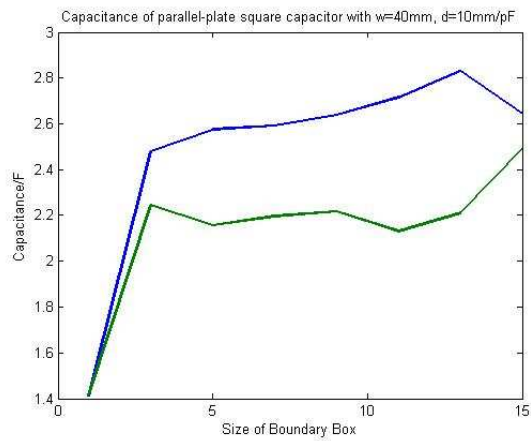


Figure 4.12: Boundary study of FEM

It's clear that capacitance value became stable and convergent to certain value after the boundary box is triple size of object. Further explanation needed to be made here is about the way HiPhi used to calculate the capacitance.

There are two ways for us to calculate the capacitance for multi-conductor systems once the field solution is known in HiPhi. One approach is to employ the automatic surface integral routines in PhiView to calculate induced charge. You must be cautious in applying surface integrals. The accuracy of the method declines significantly when electrodes have sharp corners where the electric field is effectively undefined. Also the surface integral is largely influenced by mesh size. For these situations we can get better results with volume integral methods that are less sensitive to local field interpolation errors. For a simple two-electrode system, the volume integral of field energy is related to the capacitance by Eq.(4.7), therefore we can get capacitance easily with the field energy integral. It is not difficult to extend this concept to multiple electrodes.

Another problem in AMAZE that we need to pay attention to is ResTarget index. It is the accuracy tolerance for the iterative matrix solution of the finite-element equations. HiPhi uses an iterative technique based on corrections that reduce the error in electrostatic potential at a point compared to predictions from values at neighboring nodes. The residual is an average of the relative errors over all nodes in the solution space during an iteration. This command sets a target value for the residual. The program stops if the error drops below the value. For good accuracy, the relative residual should be less than 10^{-6} . If the value of ResTarget is too low, the program may not converge because of roundoff errors. In this case, you can terminate a solution manually if you are running HiPhi in the interactive mode by using the Stop command. Default value: ResTarget = 5.0×10^{-7} .

After clarifying all the parameters we needed for simulation, the test simulation is done for parallel-plate-capacitor with different $b = d/w$. Results is shown in Fig.4.13

4.5.2 Analytic solution based BEM

Refer[45]gives an analytical solution to the calculation of capacitance of parallel square capacitor including fringe effect based on BEM numerical solutions. The mathematical formulation of the BEM is given in [11]. The parallel-plate square capacitors in an infinite

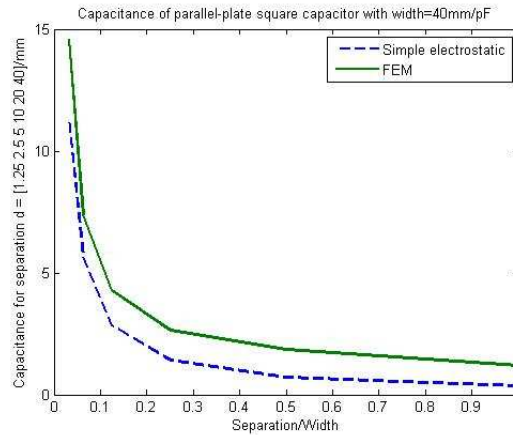


Figure 4.13: Capacitance of Parallel-plate capacitor using FEM model

space are divided into several boundary segments with equal area. In the general BEM, electrode plates are not always divided into boundary elements with equal area, but in this problem the equal division makes the numerical procedure of calculation easy and efficient. Here, the simplest approximation for the surface density charge in a boundary element is adopted. It is assumed that charge density is constant for each element (constant element method). The charge distribution on the plates of a parallel-plate square capacitor is computed. The fringe field is no longer negligible when $b = 1$, Applying regression analysis to the data of capacitance C_{BEM} - the numerical value computed by the BEM, a simple empirical expression is derived for the index represent fringe field effect,

$$\begin{cases} C_{SN} = (1 + 2.343 \cdot b^{0.891}) \cdot C & \text{when } 0.1 \leq b < 1.0 \\ C_{SN} = (1 + 2.343 \cdot b^{0.992}) \cdot C & \text{when } 1.0 \leq b \leq 10.0 \end{cases} \quad (4.9)$$

Capacitance result from BEM is shown in Fig.4.14

4.5.3 MoMtool

Fig.4.15 shows the mesh geometry constructed in MoMtool. The left figure is the initial mesh and the right figure is the mesh after adaptive refinement. The refinement steps are defined as 3 (currently limited by the memory of MATLAB). It gives information about the charge distribution on the conductor surface because of the refinement criteria we are

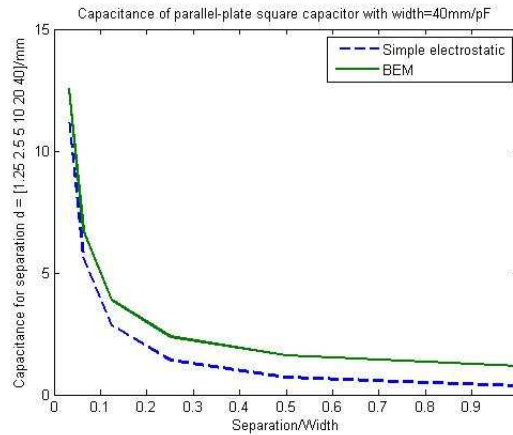


Figure 4.14: Capacitance of Parallel-plate capacitor using BEM model

Table 4.3: Capacitance of Parallel-plate Capacitor

b	$d(mm)$	$w(mm)$	$C(pF)$	$C_{SN-BEM}(pF)$	$C_{amaze-FEM}(pF)$	$C_{MoM}(pF)$
1	40	40	0.3542	1.1840	1.1854	1.3007
0.5	20	40	0.7083	1.6033	1.8431	1.7424
0.25	10	40	1.4167	2.3818	2.6431	2.6029
0.125	5	40	2.8333	3.8743	4.2633	4.2751
0.0625	2.5	40	5.6667	6.7893	7.3797	7.6705
0.03125	1.25	40	11.3337	12.5441	14.5910	13.6700

using. The objective of the refinement is to have average charge distribution for each mesh element.

Charge distribution corresponding to mesh in Fig.4.15 is shown in Fig.4.16.

To fully compare the results of above three methods, Table4.3 listed the results and Fig.4.17 shows the result of FEM, BEM and MoM tool compared to basic electrostatics formula. It's very straight forward to see how the influence of fringing fields at the edges changed corresponding to different spacing.

Fig.4.18 shows the error percentage between MoMtool and FEM, MoMtool and BEM's analytic formula. Error between MoM and BEM keeps average value as 9% and slowly decreased with the increase of spacing between two plates. This is in consistent with the fact that both MoM and BEM are integral method which holds similar principles to solve open-boundary problem. Meanwhile, the error between MoMtool and FEM is changing from

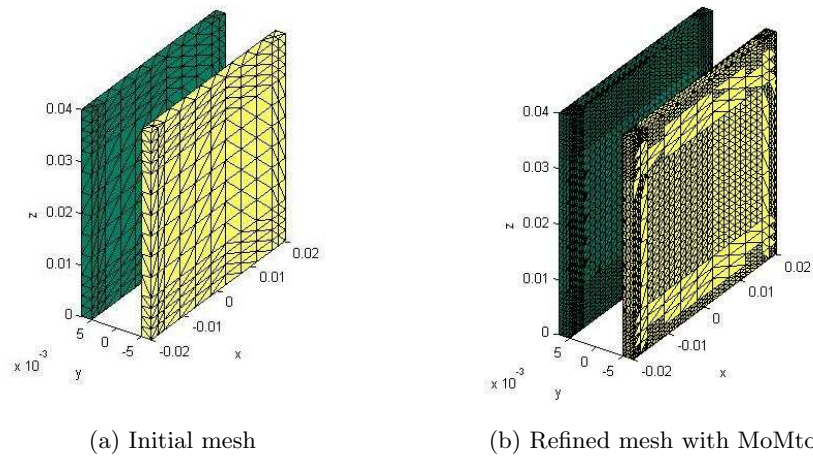


Figure 4.15: Parallel-plate Capacitor defined in MoMtool

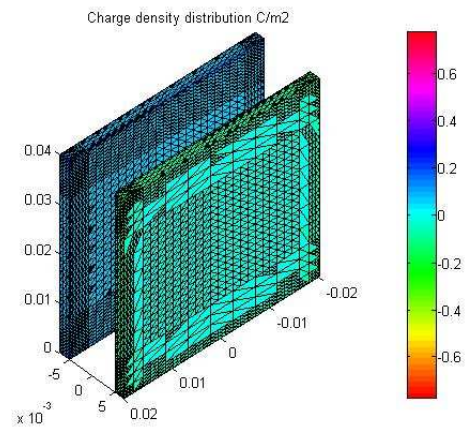


Figure 4.16: Charge density distribution of Parallel-plate Capacitor

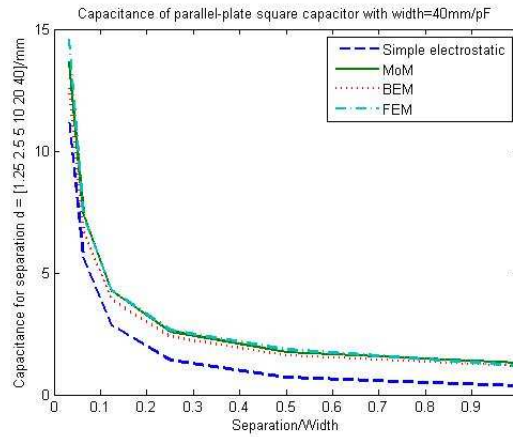


Figure 4.17: Capacitance of Parallel-plate Capacitor

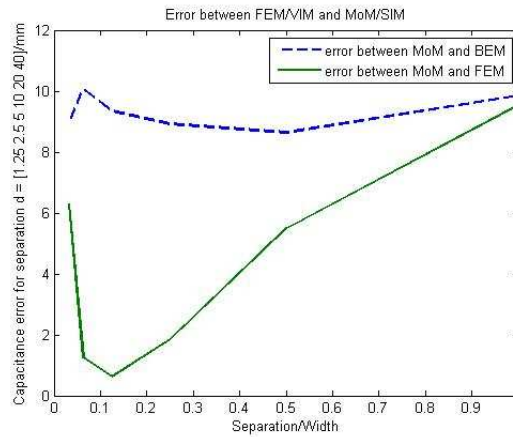


Figure 4.18: Error between different numerical results

lower than 2% to 6% corresponding to increased spacing which is also reasonable considering we are using the same boundary box for different spacing. With the increase of the spacing, the boundary box will have stronger influence on the electric field in solution volume.

As the last step, the data from MoMtool is processed. Curve fitting is employed to find the parameters of a semi-empirical parallel-plate capacitor model as Fig.4.19 shows, and possibly to improve the model itself. The criterion is the smallest RMS error. The final version of our analytical approximation reads

$$C_{MoM} = (1 + 2.83 \cdot b^{0.832}) \cdot C \quad (4.10)$$

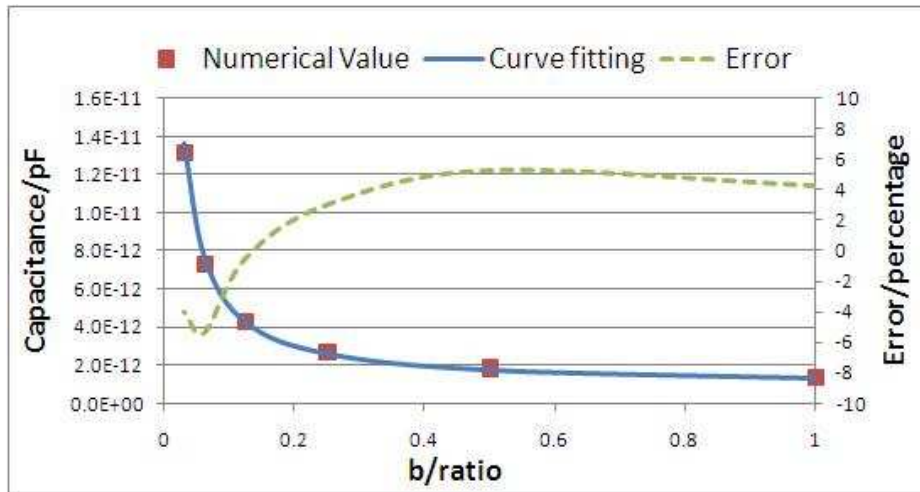


Figure 4.19: Curve fitting based on MoM result

where C is the capacitance calculated from Eq.(4.8). Since the thickness of plate has significant influence on the calculation of capacitance especially with relative small spacing shown in Fig.B.1, this solution can only be applied to parallel-plate square capacitor with 2mm thickness.

4.6 Conclusion

MoMtool employs surface integral method is an effective tool for capacitance extraction of 2D transmission line and 3D metal conductor system. The program is capable of finding the static surface charge density distribution and capacitance of any open or closed charged body having no intersecting surfaces. For the numerical examples, we have compared the capacitance matrices of an infinitely long transmission line in 2D case with that of finite-length transmission line in 3D case. We also compared our results for 3D parallel-plate capacitor with FEM method and made a conclusion that MoMtool is more convenient and efficient for open-boundary problems. The approach could easily be extended to treat intersecting surfaces and to treat the problem of determining the charge distribution when a neutrally charged object is immersed in a static electric field.

Chapter 5

Conclusion

A 3-D capacitance extraction algorithm based on Method of Moments is described. It employs simple integral calculation techniques combined with adaptive mesh refinement which leads to faster and relatively accurate solution for arbitrary 3D geometry. The method is implemented in a MATLAB-based MoMtool with a user-friendly interface. MoMtool has been applied to capacitance calculations of 3D parallel-plate capacitor and results are compared to analytic solution from simple electrostatic formula and numerical results from AMAZE utilizing Finite Element Method. It shows that even though the MoMtool utilizes single-point Gaussian integration with lower order basis function, MoMtool provides satisfied accuracy with error smaller than 5%. The results also testified the edge effects of parallel-plate capacitor increase in importance as the size of the plates is decreased compared with the spacing. Compared to FEM, the MoM is an ideal formulation for open boundary radiating structures. A major advantage of the MoM above field-based methods such as the FEM is that the free-space region between structures does not have to be discretised, this leads to faster calculation speed for simple geometry. For complex geometry with more mesh elements, solving dense non-sparse MoM matrix will create a time and memory bottleneck. Therefore, the current research interest in MoM focus on fast iterative techniques developed to efficiently solve and solve a MoM system with linear time and memory complexity as seen in QR-based approaches, FMM, and FFT-based techniques etc. Also a combination of MoM and FEM would offer the advantages of each in the appropriate regions.

Appendix A

List of Abbreviation

Table A.1: List of Abbreviation

MoM	Method of Moments
FEM	Finite Element Method
SIE	Surface Integral Equation
VLSI	Very Large-scale Integration
FDM	Finite Difference Method
BEM	Boundary Element Method
IE	Integral Equation
VIE	Volume Integral Equation
EBE	Element-by-Element
PCG	Preconditioned conjugate gradient
FMM	Fast-multiple methods
FFT	Fast Fourier Transform
MLFMA	Multilevel fast multiple algorithm
AIM	Adaptive integral method
EM	ElectroMagnetic
RF	Radio Frequency
TEM	Transverse Electromagnetic
EFIE	Electric-field integral equations
BI	Boundary Integral
BI	Boundary Integral

Appendix B

Capacitance of Parallel-plate Square Capacitor

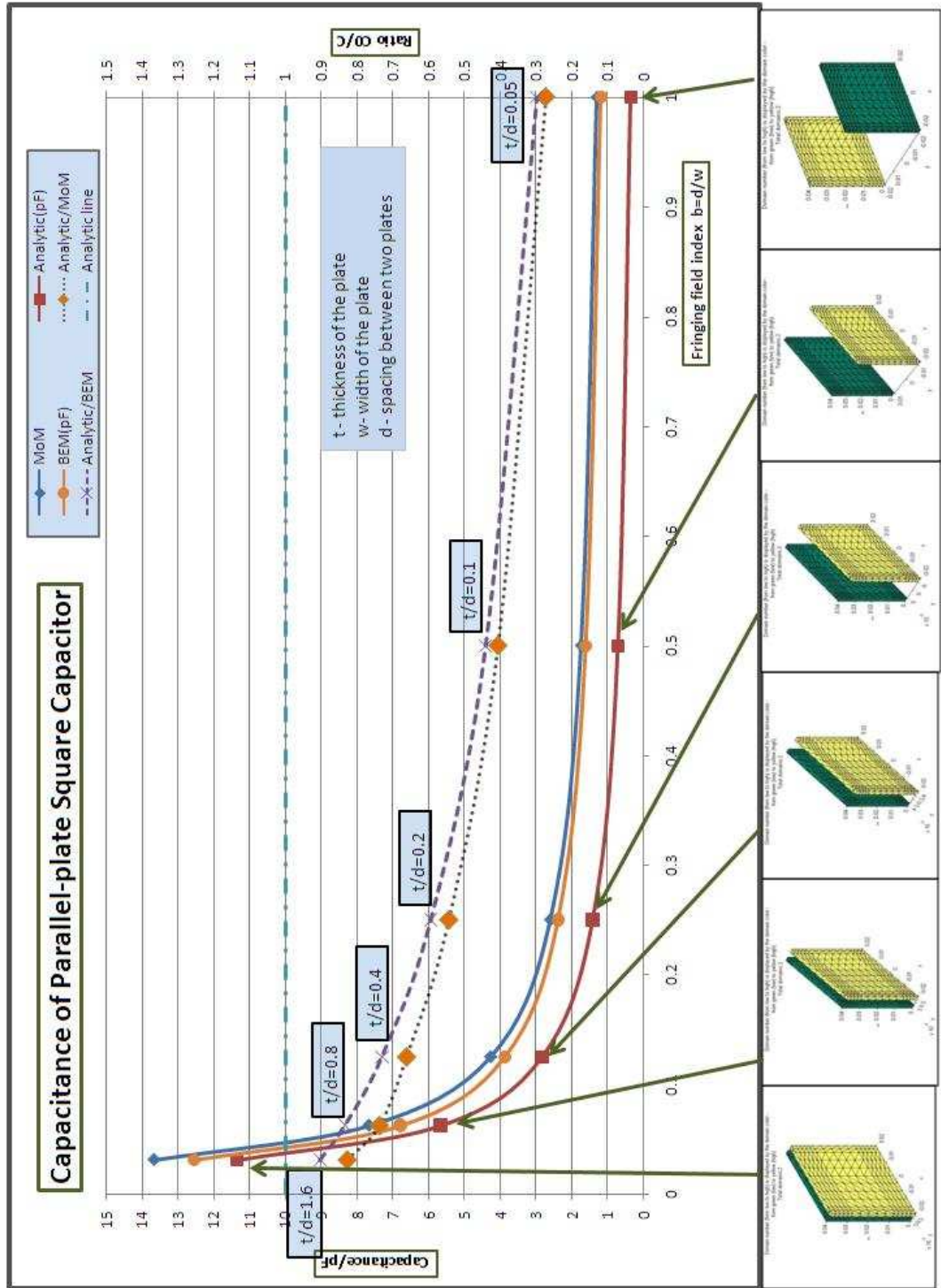


Figure B.1: Capacitance of Parallel-plate square capacitor

Bibliography

- [1] *Hiphi 2.5 three-dimensional electrostatics.*
- [2] *Matlab: The language of technical computing.*
- [3] T.Rylander A Bondeson and P. Ingelstrom, *Computational electromagnetics*, vol. 51, 2005.
- [4] P. Arcioni, M. Bressan, and L. Perregrini, *On the evaluation of the double surface integrals arising in the application of the boundary integral method to 3-d problems*, **45** (1997), 436–439.
- [5] A.Ruehli, *Circuit analysis, simulation and design*, vol. 3-part2, Amsterdam: North-Holland, 1987.
- [6] M. B. Bazdar, A. R. Djordjevic, R. F. Harrington, and T. K. Sarkar, *Evaluation of quasi-static matrix parameters for multiconductor transmission lines using galerkin's method*, **42** (1994), no. 7, 1223–1228.
- [7] Jorn Behrens and Michael Bader, *Efficiency considerations in triangular adaptive mesh refinement*, *Philosophical Transactions of The Royal Society* (2009), 4577–4589.
- [8] M. Bleszynski Bleszynski, E. and T.Jaroszewicz, *Aim: Adaptive integral method for solving large-scale electromagnetic scattering and radiation problems*, *Radio Science* **31** (1996), 1225–1251.
- [9] A. Brandt, *Multilevel computations of integral transformations and partial interactions with oscillatory kernel*, *Comput. Phys. Commun.* **65** (1991), no. 1-3, 24–38.

- [10] P.-S. Kooi C.-F. Wang, L.-W. Li and M.-S. Leong, *Efficient capacitance computation for three-dimensional structures based on adaptive integral method*, Progress In Electromagnetics Research **30** (2001), 3346.
- [11] J.C.F.Telles C.A.Brebbia and L.C.Wrobel, *Boundary element techniques - theory and applications in engineering*, Berlin: Springer, New York, 1984.
- [12] A. C. Cangellaris, *Distributed equivalent sources for the analysis of multiconductor transmission lines excited by an electromagnetic field*, **36** (1988), no. 10, 1445–1448.
- [13] Y.C.Wong C.N.Chang and C.H.Chen, *Hybird quasistatic analysis for multilayer coplanar lines*, IEE Proc.-H **138** (1991), 307–312.
- [14] D.M.Pozar, *Microwave engineering*, 3 ed., New York, 2005.
- [15] Sophie Loire Dong Eui Chang¹ and Igor Mezi²c, *Closed-form solutions in the electrical field analysis for dielectrophoretic and travelling wave inter-digitated electrode arrays*, Journal of physics: Applied physics (2003), 3073–3078.
- [16] T. F. Eibert and V. Hansen, *On the calculation of potential integrals for linear source distributions on triangular domains*, **43** (1995), no. 12, 1499–1502.
- [17] O. Ergul and L. Gurel, *Comparison of integral-equation formulations for the fast and accurate solution of scattering problems involving dielectric objects with the multilevel fast multipole algorithm*, **57** (2009), no. 1, 176–187.
- [18] A. Farrar and A. T. Adama, *Computation of lumped microstrip capacitances by matrix methods-rectangular sections and end effect*, IEEE Trans. Microwave Theory Tech **MTT-19** (1971), 495–497.
- [19] F.Ulaby, *Fundamental of applied electromagnetics*, 5 ed., Prentice Hall, Upper Saddle River, 2007.
- [20] Ramesh Garg, *Analytical and computational methods in electromagnetics*, Artech House Inc., 2008.

- [21] S. G. Gaskill, V. S. Shilimkar, and A. Weisshaar, *Accurate closed-form capacitance extraction formulas for metal fill in rfics*, (2009), 611–614.
- [22] Dipanjan Gope and Vikram Jandhyala, *Pilot: A fast algorithm for enhanced 3d parasitic capacitance extraction efficiency*, *Microwave and optical technology letters* **41** (2004), 169–173.
- [23] R. D. Graglia, *On the numerical integration of the linear shape functions times the 3-d green's function or its gradient on a plane triangle*, **41** (1993), no. 10, 1448–1455.
- [24] L. Greengard and V. Rokhlin, *A fast algorithm for particle simulations*, *Journal of Computational Physics* (1987), 73(2):325–348.
- [25] Chang-Hoi Ahn Han Kim, *Mfma for capacitance extraction using adaptive triangular mesh*, *Proceedings of APMC2001* (2001), 87–90.
- [26] R. F. Harrington, *Losses on multiconductor transmission lines in multilayered dielectric media*, **32** (1984), no. 7, 705–710.
- [27] Chapel Hill, *Efficient galerkin techniques for multipole-accelerated capacitance extraction of 3-d structures with multiple dielectrics*, 16th Conference on Advanced Research in VLSI, 1995.
- [28] R. Hiptmair and O. Sterz, *Current and voltage excitations for the eddy current model*, *Int. J. Num Modeling: Electronic networks, Devices, and Fields* **18** (2005), 1–21.
- [29] W. Hong, W. Sun, Z. Zhu, H. Ji, B. Song, and W. Wei-Ming Dai, *A novel dimension reduction technique for the capacitance extraction of 3d vlsi interconnects*, *Proc. IEEE/ACM International Conference on Computer-Aided Design ICCAD-96. Digest of Technical Papers*, November 10–14, 1996, pp. 381–386.
- [30] J.C.Maxwell, *A treatise on electricity and magnetism*, New York: Dover Publications, 1954.
- [31] J.D.Jackson, *Claasical electrodynamics*, New York, 1982.

- [32] D. C. Jiles, *Modelling the effects of eddy current losses on frequency dependent hysteresis in electrically conducting media*, **30** (1994), no. 6, 4326–4328.
- [33] Pei Jinming, Zhu Shouzheng, and An Tongyi, *Transient analysis of lossy multiconductor transmission line in multilayered dielectric media under interfering field*, Proc. (ICCEA '99) 1999 International Conference on Computational Electromagnetics and Its Applications, 1999, pp. 383–385.
- [34] Y. Kamen and L. Shirman, *Triangle rendering using adaptive subdivision*, **18** (1998), no. 2, 95–103.
- [35] D. W. Kammler, *Calculation of characteristic admittances and coupling coefficients for strip transmission lines*, **16** (1968), no. 11, 925–937.
- [36] M. Kamon, M. J. Tsuk, and J. K. White, *Fasthenry: a multipole-accelerated 3-d inductance extraction program*, **42** (1994), no. 9, 1750–1758.
- [37] S. Kapur and D. E. Long, *Ies3: a fast integral equation solver for efficient 3-dimensional extraction*, (1997), 448–455.
- [38] B. M. Kolundzija and V. V. Petrovic, *Comparison of mom/sie, mom/vie and fem based on topological analysis of two canonical problems*, **1** (1998), 274–277 vol.1.
- [39] S. Kulkarni, R. Lemdiasov, R. Ludwig, and S. Makarov, *Comparison of two sets of low-order basis functions for tetrahedral vie modeling*, **52** (2004), no. 10, 2789–2795.
- [40] Gtz Leonhardt, *Static inductance extraction by means of the monte carlo method and comparison with related approaches*, Ph.D. thesis, Swiss Federal Institute of Technology Zurich, 2000.
- [41] C.F.Wang Ling, F. and J.M.Jin, *Application of adaptive integral method to scattering and radiation analysis of arbitrarily shaped planar structures*, J. Electromagn. Waves Appl **12** (1998), 1021–1037.
- [42] S. N. Makarov and R. Ludwig, *Analytical model of the split-coaxial balun and its application to a linearly-polarized dipole or a cp turnstile*, **55** (2007), no. 7, 1909–1918.

- [43] K. Nabors, S. Kim, and J. White, *Fast capacitance extraction of general three-dimensional structures*, **40** (1992), no. 7, 1496–1506.
- [44] K. Nabors, S. Kim, J. White, and S. Senturia, *Fast capacitance extraction of general three-dimensional structures*, Proc. IEEE International Conference on Computer Design: VLSI in Computers and Processors ICCD '91, October 14–16, 1991, pp. 479–484.
- [45] H. Nishiyama and M. Nakamura, *Form and capacitance of parallel-plate capacitors*, IEEE Transactions on Components, Packaging, and Manufacturing Technology, Part A **17** (1994), no. 3, 477–484.
- [46] A.J. van Genderen N.P.van der Meijs, *An efficient finite element method for submicronic capacitance extraction*, 26th ACM/IEEE Design Automation Conference, 1989.
- [47] A.J.van Genderen N.P.van der Meijs, *Delayed frontal solution for finite-element based resistance extraction*, Proceedings of the 32nd Design Automation Conference, ACM (San Francisco, CA, USA), ACM, 1995, pp. 273–278.
- [48] R. G. Olsen, *Power-transmission electromagnetics*, **36** (1994), no. 6, 7–16.
- [49] P. D. Patel, *Calculation of capacitance coefficients for a system of irregular finite conductors on a dielectric sheet*, **19** (1971), no. 11, 862–869.
- [50] J. R. Phillips and J. K. White, *A precorrected-fft method for electrostatic analysis of complicated 3-d structures*, **16** (1997), no. 10, 1059–1072.
- [51] S. Rao, A. Glisson, D. Wilton, and B. Vidula, *A simple numerical solution procedure for statics problems involving arbitrary-shaped surfaces*, **27** (1979), no. 5, 604–608.
- [52] D. K. Reitan, *Accurate determination of the capacitance of rectangular parallel-plate capacitors*, J. Appl. Phys. **30** (1959), 172–176.
- [53] A. Ruehli, *Electrical analysis of interconnections in a solid state circuit environment*, Proc. Solid-State Circuits Conference. Digest of Technical Papers. 1972 IEEE International, vol. XV, 1972, pp. 64–65.

- [54] A. E. Ruehli and P. A. Brennan, *Efficient capacitance calculations for three-dimensional multiconductor systems*, **21** (1973), no. 2, 76–82.
- [55] J. Whinnery S. Ramo and T.v. Duzer, *Fields and waves in communication electronics*, New York:John Wiley& Sons Inc, 1965.
- [56] T. K. Sarkar and R. F. Harrington, *The electrostatic field of conducting bodies in multiple dielectric media*, **32** (1984), no. 11, 1441–1448.
- [57] M. S. Sharawi and D. N. Aloï, *Design of linearly polarized rectangular patch antenna using mom, ftd and fem*, Proc. IEEE Antennas and Propagation Society International Symposium, 2007, pp. 3916–3919.
- [58] J. Song, Cai-Cheng Lu, and Weng Cho Chew, *Multilevel fast multipole algorithm for electromagnetic scattering by large complex objects*, **45** (1997), no. 10, 1488–1493.
- [59] J.M. Song and W.C. Chew, *Fast multiple method solution using parametric geometry*, Microwave Opt. Tech. Lett **7** (1994), no. 16, 760–765.
- [60] F. Ling J.M.Song Wang, C.F. and J.M.Jin, *Adaptive integral solution of combined field integral equation*, Microwave Opt. Tech. Lett **19** (1998), 321–328.
- [61] Zhongde Wang, J. Volakis, K. Saitou, and K. Kurabayashi, *Comparison of semi-analytical formulations and gaussian-quadrature rules for quasi-static double-surface potential integrals*, **45** (2003), no. 6, 96–102.
- [62] W. T. Weeks, *Calculation of coefficients of capacitance of multiconductor transmission lines in the presence of a dielectric interface*, **18** (1970), no. 1, 35–43.
- [63] C. Wei and R.F.Harrington, *Computation of the parameters of multiconductor transmission lines in two dielectric layers above a ground plane*, Depart. Electrical Computer Eng., Syracuse Univer. (1982).
- [64] Cao Wei, R. F. Barrington, J. R. Mautz, and T. K. Sarkar, *Multiconductor transmission lines in multilayered dielectric media*, **32** (1984), no. 4, 439–450.

- [65] Hongchuan Wei, Guanghui Wang, and Zeyi Wang, *Coupling computation of the bem and fdm in 3d capacitance extraction*, Proc. 4th International Conference on ASIC, 2001, pp. 716–719.
- [66] D. Wilton, S. Rao, A. Glisson, D. Schaubert, O. Al-Bundak, and C. Butler, *Potential integrals for uniform and linear source distributions on polygonal and polyhedral domains*, **32** (1984), no. 3, 276–281.
- [67] Charles W. Steele, *Numerical computation of electric and magnetic fields*, New York: Van Nostrand Reinhold, 1987.
- [68] Jianfeng Xu, Wen-Yan Yin, and J. Mao, *Capacitance extraction of high-density 3d interconnects using finite element method*, Proc. Asia-Pacific Microwave Proceedings APMC 2005, vol. 2, December 4–7, 2005, p. 3pp.
- [69] A. H. Zemanian, R. P. Tewarson, C. P. Ju, and J. F. Jen, *Three-dimensional capacitance computations for vlsi/ulsi interconnections*, **8** (1989), no. 12, 1319–1326.
- [70] Wei Zhuang, *A 3-d capacitance extraction algorithm based on kernel independent hierarchical method and geometric moments*, Master’s thesis, Texas A&M University, 2006.